Biomechanical Characterization of Crystalline Lens by Optical Coherence Elastography

by
Hongqiu Zhang

A dissertation submitted to the Department of Biomedical Engineering,
Cullen College of Engineering
in partial fulfillment of the requirements for the degree of

Doctor of Philosophy

in Biomedical Engineering

Chair of Committee: Kirill V. Larin

Committee Member: Salavat R. Aglyamov

Committee Member: Jerome S. Schultz

Committee Member: Fabrice Manns

Committee Member: Yingchun Zhang

University of Houston
December 2021

ACKNOWLEDGEMENTS

Five years is a long time. I spent all my efforts chasing for my Ph. D degree. During this long but exciting journey, I have got help from a lot of people. I want to thank you all for helping me with everything you gave me. I will give my biggest thanks to Professor Kirill V. Lain, my supervisor, for your supervision. Your honest, caring and wise choice helped me to get the right direction in chasing my degree. Your unstopped passion and smart ideas always make me inspired. I understand this is how a great professor should be like. It is my life-long fortune to digest everything you taught me in these years.

I want to thank my dissertation committee, Professor Salavat R. Aglyamov, Professor Jerome S. Schultz, Professor Fabrice Manns, and Professor Yingchun Zhang, for their assistance throughout my dissertation work.

I want to thank Professor Salavat R. Aglyamov and Professor Jerome S. Schultz for their daily help with my projects. I cannot get every single achievement without your help. I want to thank Dr. Manmohan Singh, Dr. Jose Fernando Zvietcovich, and Dr. Behzad Khajavi for your help with my programming and system building. I always learn new things from you. You are as friendly as my brothers.

I want to thank all my colleagues and friends from the Biomedical Optics Laboratory. I appreciate Dr. Chen Wu, Dr. Chih-Hao Liu, Dr. Raksha Raghunathan for their nice guidance and suggestions when I joined the group. I also thank Dr. Alexander Schill, Achuth Nair, Justin Rippy, Harshdeep Singh Chawla, Yogeshwari Ambekar for your friendship and help. None of my work can be achieved without any of you guys.

I owe my thanks to my father and mother. I left my hometown, and it has been five years. I have not got a chance to go back to see you. My missing towards you is one of my most important reasons for staying here and finishing my program. Finally, many thanks to my passed-away grandfather and grandmother, my uncles and aunts, and all my relatives, for your consistent help and support. I have nothing to pay back but my hard work and my great job on my Ph. D. project.

ABSTRACT

This dissertation reports on the application of optical coherence tomography (OCT) based elastography technique to assess the biomechanical properties of crystalline lens tissue noninvasively quantitatively. This work is summarized in four sections: 1) Assessing the Effects of Storage Medium on the Biomechanical Properties of Porcine Lens with Optical Coherence Elastography; 2) Optical Coherence Elastography of Cold Cataract in Porcine Lens; 3) The Mechanical Properties of Oxidative Cataract and the Potential Medical Treatment Measured by Optical Coherence Elastography; 4) Age-Related Changes in Rabbit Lens Viscoelasticity by Surface Wave Dispersion Analysis. These methods and applications are demonstrated with experiments on both tissue-mimicking phantoms (gelatin and agar) and lens (porcine and rabbit) *ex vivo* and *in situ* under different conditions (medium preservation, cold cataract, oxidative cataract, aging). This dissertation represents the frontier and emerging research area of noninvasive optical coherence elastography. It is expected to contribute to the field of quantitative biomechanical assessment with research and clinical-based applications.

TABLE OF CONTENTS

ACKNOWLEDGMENTS ..... **iii**

ABSTRACT ..... **v**

TABLE OF CONTENTS ..... **vi**

LIST OF TABLES ..... **viii**

LIST OF FIGURES ..... **ix**

I. INTRODUCTION AND BACKGROUND **1**

I.1 Crystalline Lens 1

I.2 Biomechanical Tissue Characterization 1

I.3 Lenticular Biomechanical Properties 2

I.4 Common Elastography Methods 4

I.5 Optical Coherence Tomography (OCT) 6

I.5.1 Spectral-domain OCT (SD-OCT) 8

I.5.2 Swept-source OCT (SS-OCT) 9

I.5.3 Phase Sensitive OCT (PhS-OCT) 10

I.6 Optical Coherence Elastography (OCE) 11

I.7 Shear Wave Model 12

I.8 Organization of This Dissertation 13

II. ASSESSING THE EFFECTS OF STORAGE MEDIUM ON THE BIOMECHANICAL PROPERTIES OF PORCINE LENS WITH OPTICAL COHERENCE ELASTOGRAPHY **15**

II.1 Introduction 15

II.2 Materials and Methods 16

II.3 Results 18

II.4 Discussion 21

II.5 Conclusion and Future Work 22

III. OPTICAL COHERENCE ELASTOGRAPHY OF COLD CATARACT IN PORCINE LENS **23**

III.1 Introduction 23

III.2 Materials and Methods 26

III.3 Results 29

III.4 Discussion 37

III.5 Conclusion 40

IV. ELASTICITY CHANGES IN THE CRYSTALLINE LENS DURING OXIDATIVE DAMAGE AND THE ANTIOXIDANT EFFECT OF ALPHA-LIPOIC ACID MEASURED BY OPTICAL COHERENCE ELASTOGRAPHY ……..41

IV.1 Introduction.....41

IV.2 Materials and Methods 43

IV.2.1 Experimental Set-up 43
IV.2.2 Sample Preparation.....44
IV.2.3 Optical Properties Measurements 45
IV.2.4 Surface Wave Measurements 46

IV.3 Results.....47

IV.3.1 Lens Transparency Analysis.....47
IV.3.2 OCE Measurement of the Lenticular Biomechanical Properties....49

IV.4 Discussion.....53

IV.5 Conclusion 56

V. AGE-RELATED CHANGES IN THE VISCOELASTICITY OF RABBIT LENS CHARACTERIZED BY SURFACE WAVE DISPERSION ANALYSIS 57

V.1 Introduction.....57

V.2 Materials and Methods.....59

V.2.1 Experimental Setup 59
V.2.2 Sample Preparation 62
V.2.3 Wave Propagation Model.....63

V.3 Results.....64

V.4 Discussion 73

V.5 Conclusion 76

VI. CONCLUSION.....77

REFERENCES.....78

APPENDICES

JOURNAL PUBLICATION WITH AUTHORSHIP.....103

LIST OF TABLES

4.1 The Young's modulus of the lenses by mechanical testing and OCE.....53

5.1 The size and mass of the rabbit lenses.....64

LIST OF FIGURES

1.1 Cross-sectional schematic of a human lens 4

1.2 Schematic of a typical SD-OCT system 9

1.3 Schematic of a typical SS-OCT system 10

2.1 Schematic of the experimental setup 16

2.2 The estimated Young's modulus of the lenses incubated in the different indicated media over 24 hours (N=3 for each medium) 19

2.3 The estimated Young's modulus of the lenses incubated in M-199 medium at 4°C, 22°C, and 37°C over 12 hours (N=3 for each temperature) 20

2.4 The estimated Young's modulus of the lenses incubated in M-199 media at various pHs over 24 hours (N=3 for each pH) 21

3.1 Schematic of the experimental setup during the OCE measurements 26

3.2 The OCE-measured group velocity in a 3% gelatin and 1% agar phantoms as a function of temperature. 30

3.3 Images from a dissecting microscope while a fresh porcine lens was (a) cooled from 21°C to 6°C and (b) warmed from 6°C to 21°C after being in a 4°C refrigerator for 6 h 32

3.4 OCT structural images of a fresh porcine lens that was (a) cooled from 21°C to 6°C and (b) warmed from 6°C to 21°C after being in a 4°C refrigerator for 6 h 34

3.5 The measured group velocities and estimated Young's moduli for the fresh lenses and lenses with induced cold cataracts. 35

4.1 The Schematic of the OCE system 44

4.2 Photos of the lenses as a function of time and incubation media 48

4.3 The attenuation calculated from the OCT images of the lenses incubated with five different media 49

4.4 Space-time maps of one (**a**) H_2O_2→PBS and (**b**) H_2O_2→ALA lens at nine hours 50

4.5 The surface wave group velocities measured in the lenses incubated with five different media. 51

4.6 The OCE-estimated Young's moduli for the lenses incubated with five different media 52

5.1 Schematic of the *in situ* US-OCE system 60

5.2 Schematic of the *ex vivo* air-coupled US-OCE system 61

5.3 The OCT image of the lens *in situ* 62

5.4 OCE-measured dispersion curves for the elastic wave propagation at the lens surface and (red line) fitting by the Scholte wave model for (a) one young lens and (b) one mature lens. 65

5.5 Average elastic wave dispersion curves of the young (N=5) and mature (N=10) lenses and the fit to the mechanical model using Eq. 5.1. 66

5.6 (a) Young's modulus and (b) shear viscosity coefficient of the young and matured lenses estimated based on the viscoelastic model. 67

5.7 (blue circles) OCE-measured dispersion curves for the elastic wave propagation at the lens surface and (red line) fitting for one young lens (a) inside the eyeball and (b) outside the eyeball. 68

5.8 The estimated phase velocity dispersion curves of the young lens inside and outside the eyeball. 69

5.9 The (a) Young's modulus and (b) shear viscosity of the young lenses estimated based on Scholte wave model and Rayleigh wave model. 70

5.10 (blue circles) OCE-measured dispersion curves for the elastic wave propagation at the lens surface and (red line) fitting for one mature lens (a) inside the eyeball and (b) outside the eyeball. 71

5.11 The estimated phase velocity dispersion curves of the mature lens inside and outside the eyeball. 72

5.12 The (a) Young's modulus and (b) shear viscosity of the mature lenses estimated based on Scholte wave model and Rayleigh wave model. 73

CHAPTER I – Introduction and Background

I.1 Crystalline Lens

The crystalline lens is critical to the focusing ability of the human eye responsible for the accommodation process [1]. To a large extent, the capacity of the lens to change refractive power is affected by the aging process or eye diseases [2, 3]. The biomechanical properties of the lens usually change with age (presbyopia) or during certain diseases, such as cataract [4, 5]. These conditions cause the lenticular biomechanical properties to change significantly, including increased stiffness and reduced ability of the ciliary muscle to control accommodation, which lead the eye to be unable to focus light on the retina when looking at close objects [6, 7]. Our current understanding of the mechanical properties of the lens, their changes with age, and their role in presbyopia and cataract is limited, in part due to a lack of technology that allows measurements of the mechanical properties of the lens *in situ* and *in vivo*. Analysis of the lens can be challenging because it is difficult to reach directly. Noninvasive techniques are developed to indirectly investigate the bio-tissues without any disturbance to the physiology of the patients. The ability to noninvasively measure biomechanical properties of the crystalline lens *in vivo* will allow direct objective evaluation of the outcomes of techniques to restore accommodation that rely on lens softening, including femtosecond lasers, pharmaceutical agents, or lens replacement with a flexible material [8-14].

I.2 Biomechanical Tissue Characterization

Tissue characterization is critical in understanding the functions of different biological tissues in the human body [15]. In the medicine field, tissue characterization is fundamental, especially during surgery and disease assessment. For instance, myocardial

tissue characterization through LGE and TI-weighted imaging has an enormous clinical role in assessing ischemic heart illness and non-ischemic myocardial infections [16]. Furthermore, accurate tissue characterization is essential for scientists and doctors to understand the human body more accurately, leading to more remarkable advancements for human healthcare [17]. For example, the refractive index of the crystalline lens is essential to myopia research [18].

Among tissue characterization methods, tissue biomechanical characterization is crucial for researchers to understand tissue mechanical functions. Since lenticular biomechanical properties are critical for the vision, as written in Section I.1, the accurate quantification would help people understand more about myopia, cataract, and presbyopia, or other conditions and develop the related treatments of those conditions [19].

In order to investigate the biomechanical properties of the biological tissues, different noninvasive methods are utilized, such as radiology, acoustics, and electromagnetics [20]. Based on the published results, it is clear that the elastic properties are significantly different among different types of tissues [21-23]. The understanding of the elasticity variations can improve the accuracy of the characterization of different tissues. In this dissertation, my work combines optics and mechanics to make the new applications on optical coherence tomography-based elastography for quantitatively characterizing the lens tissue.

I.3 Lenticular Biomechanical Properties

Figure 1.1 shows the cross-sectional schematic of a crystalline lens. The structure of a crystalline lens contains four parts: capsule, epithelium, cortex, and nucleus. Among them,

the lens capsule is an uninterrupted basement membrane for sequestering it from the other ocular tissues and protecting it from the pathogen [24]. The capsule of the lens provides a suitable environment for the lens cells [25], storing and releasing sequestered growth factors [26] and supporting and transporting the metabolites of the lens [27]. The lens epithelium cells are in the anterior portion of the lens capsule, and it majorly regulates most of the homeostatic functions of the lens [28]. The lens cortex is the tissue surrounding the lens nucleus, and the lens nucleus is the core of the lens. The crystalline lens contains different kinds of crystallin proteins, categorized as α-crystallin, β-crystallin, and γ-crystallin [29]. The β- and γ-crystallin protein construct the structure of the lens fibers and make it elastic and viscous inside the eyeball while α-crystallin works as the chaperone for β- and γ-crystallin protein to prevent their further precipitation and lens opacity [30]. Since both the cortex and the nucleus are constructed by lens fiber cells, there are no clear boundaries [31].

Generally, the elasticity of the lens changes from the capsule to the nucleus and increases during the aging process [32]. The viscosity of the lens tends to increase during the aging process, but the accommodation capacity of the lens with age tends to decrease [33]. The nucleus is the stiffest part for the old lens, but the cortex is the stiffest part for the young lens [34]. The cold cataract and the age-related cataract usually happen in the nucleus [35, 36].

Investigations show that the porcine lens is viscoelastic and readily deformed [37]. The porcine and rabbit lenses are similar to human lenses in size and have similar shear moduli. Therefore, these lenses are good models to investigate the human lens since understanding

the lens's viscoelastic properties can directly impact the investigation of lens deformation and accommodation. This dissertation discusses the porcine lens, rabbit lens, and their roles in investigating the human lens in viscoelasticity research.

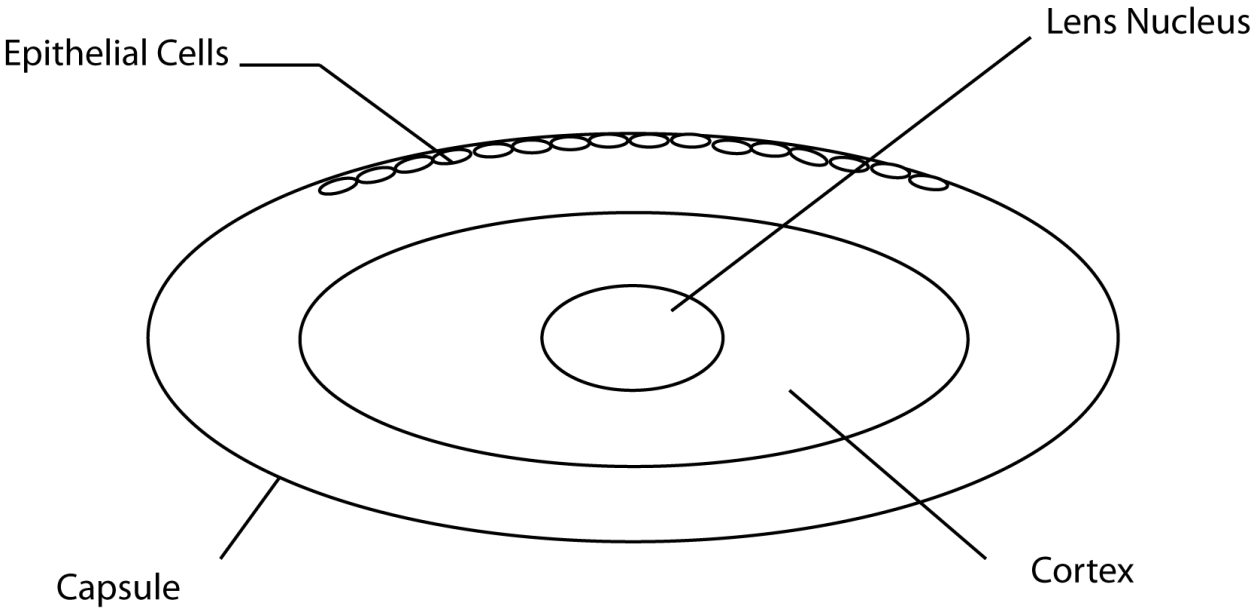

Figure 1.1 Cross-sectional schematic of a human lens

I.4 Common Elastography Methods

There are different techniques developed to investigate the biomechanical properties. For example, ultrasound elastography utilizes stiffness as the imaging principle [38, 39]. Some X-ray-based imaging technology such as X-ray and computed tomography (CT) [40, 41] can be applied to investigate the tissue biomechanical properties as well [42]. Magnetic Resonance Elastography (MRE) started to be accepted by orthopedists in detecting biomedical property changes such as muscle and ligament problems [43-45]. It is essential to note that MRE and ultrasound elastography are noninvasive *in vivo* diagnostic methods [39, 46, 47]. However, since some of the techniques can cause permanent damages to the human eye or do not have resolution high enough, the noninvasive technique utilized on lenticular biomechanical properties should be properly selected.

In the specific field of measuring the lenticular biomechanical properties, the biggest concern is that the method needs to measure the lenticular properties noninvasively. Ultrasound elastography, magnetic elastography, and supersonic shear imaging are promising noninvasive methods for lens and cornea [48-50]. However, some of the methods require a large amplitude to excite the tissue due to their low sensitivity to small displacements. Moreover, because the lens is located inside the globe of the eye, between the aqueous and vitreous humors, it is not practical to utilize invasive methods to measure the lenticular mechanical properties.

Some newly developed methods are applicable in investigating the biomechanical properties of the lens *in vivo*. Brillouin microscopy is a promising method in achieving the depth-dependent biomechanical properties in the crystalline lens *in vivo* and providing high-resolution 3D elasticity maps of the lens [51, 52]. Though Brillouin microscopy can measure the biomechanical properties without any external excitation based on Brillouin scattering, the quantitative approach applied for the viscoelasticity of the tissue still needs more investigation, which means the quantification of lenticular viscoelasticity by Brillouin spectroscopy (Brillouin system) is still not fully known [53].

Optical Coherence Tomography (OCT) is a promising, noninvasive, rapid, high-resolution technique, and widely used in ophthalmology [54-56]. As the OCT-based elastography can rapidly, noninvasively, and with high micrometer-scale spatial resolution, OCT-based elastography can be utilized to measure the lens's biomechanical properties. This dissertation examines its application for the noninvasive assessment of lenticular biomechanical properties.

I.5 Optical Coherence Tomography (OCT)

Optical coherence tomography (OCT) is a noninvasive imaging technique for high-resolution images in two or three dimensions. OCT allows one to evaluate tissue's scattering and absorption properties *in vivo* with a penetration depth of 1~3 mm [15]. It was introduced for the cross-sectional image of the retina with micron-scale axial resolution [57]. Since James G. Fujimoto, Adolf F. Fercher, Christoph K. Hitzenberger, David Huang, and Eric A. Swanson developed this technology 30 years ago [57], it has been applied in many clinical areas, such as corneal imaging, angiography, tumor imaging, dermatology, and elastography [23, 58-62]. In 1992, a startup firm called Advanced Ophthalmic Devices, which grew from MIT, introduced the OCT system as an ophthalmological imaging technique. OCT can be utilized to do research on lenticular studies with further development, especially on lenticular biomechanical properties [63-67].

In general, OCT offers three significant advantages on different applications, especially for lenticular applications:

1) High data acquisition speed. With the fast-speed development of laser hardware, OCT primarily relates its light source and recurrent technological advancements, including double buffering, scan clock gating, and direct display that has led to the creation of high-speed systems [68]. The speed of the newest ultrafast OCT system can reach 400 million A-lines per second [69].
2) High spatial resolution. The axial resolution of OCT can be expressed based on the central wavelength and the bandwidth of the light source [70]:

$$\delta_z = l_c = \frac{2\ln(2)}{\pi}\frac{\lambda_0^2}{\Delta\lambda} \quad (1.1)$$

where λ_0 is the central wavelength of the light source, and $\Delta\lambda$ is the full-width half max (FWHM) of the light source. Eq. 1.1 shows how the light source affected the axial resolution, including its central wavelength and bandwidth. OCT applies light sources that usually have a bandwidth of 80~150 nm, which leads to the axial resolution of less than 10 μm.

3) Millimeter-long penetration depth. OCT imaging technique originated from low coherence interference (LCI). The near-infrared light with wavelength between 800 nm and 1700 nm makes OCT show the about 1~3 mm depth in the high-scattering biological tissues with high-resolution in cross-section view [71].

Generally, if the central wavelength of the light source is shorter, the axial resolution will be higher, and broader bandwidth can result in an even higher axial resolution. The wavelength of the light usually ranges between 800 nm and 1300 nm. There is a significant tradeoff between axial resolution and penetration depth.

Time-domain OCT is the first generation of OCT [57]. It is developed to detect back-scattered photons from the tissue of interest with a coherence length of the source with a two-beam interferometer. The improved OCT system is called Fourier-domain OCT [72]. The frequency modulation spectrally encodes its depth information on the interference spectrogram, and Fourier Transform processed the reconstruction of the images to provide depth information. FD-OCT is further developed into two schemes: Spectral Domain OCT (SD-OCT) and Swept Source OCT (SS-OCT). They are also called optical frequency

domain imaging. They are different in the method of construction of the spectrogram and the components employed.

I.5.1 Spectral-domain OCT (SD-OCT)

In FD-OCT systems, like SD-OCT, the imaging depth relies on the wavelength information, the same as the TD-OCT system. Instead of a photodetector, a high-speed line-scan CCD camera is part of the spectral-domain OCT. The captured fringe works as a spectrum of the interference signal. Fig 1.2 shows the schematic of an SD-OCT system. The fringe signal detected by the CCD camera complies with the equation [73]:

$$I(k) = s(k)\sqrt{I_1 I_2}\cos(2nk\Delta x) \tag{1.2}$$

where $k = \frac{2\pi}{\lambda}$ is the wavenumber (the spatial frequency of a wave), λ is the wavelength, $I(k)$ is the intensity of the interference signal by the wavenumber k, $s(k)$ is the light source spectrum. With a 50/50 beam splitter, the reference arm and the sample arm should have the same spectrum. For the particular wavenumber k, I_1 is the intensity from the sample arm and I_2 is the intensity from the reference arm. $n\Delta x$ is the pathlength between the two arms, regulated by the refractive index n. After a Fourier Transform is performed, the fringes can be transformed to proper A-lines.

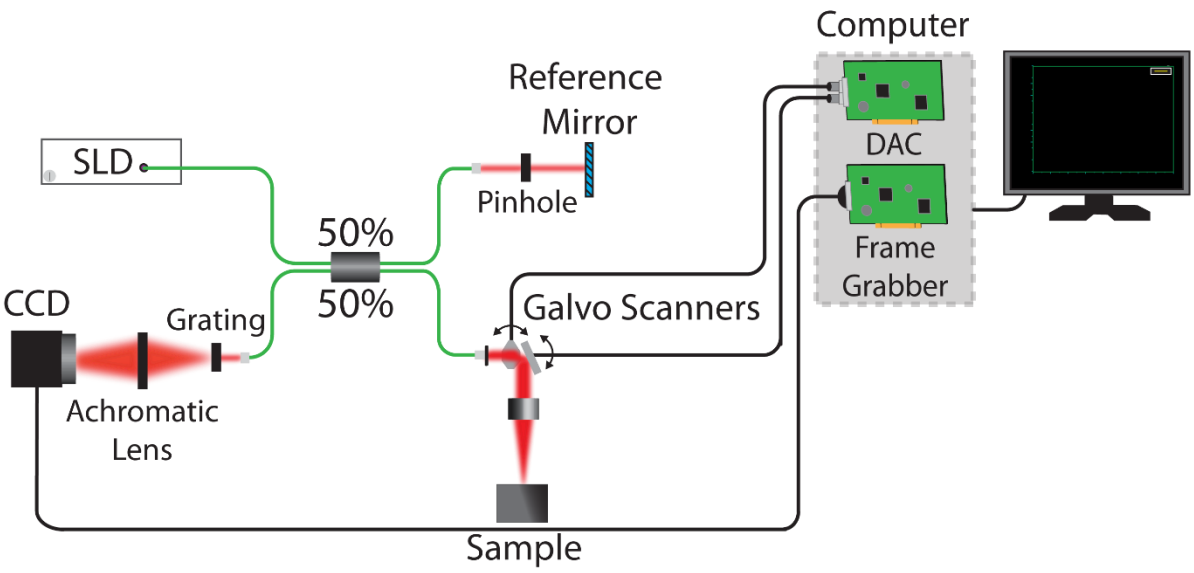

Figure 1.2 Schematic of a typical SD-OCT system

I.5.2 Swept-source OCT (SS-OCT)

The OCT system based on the swept-source laser is called swept-source OCT (SS-OCT). Fig 1.3 shows the schematic of an SS-OCT system. The light from the broadband laser is split into the sample arm and reference arm. After the reference arm reflection and the sample arm scattering, the returning light from both arms is coupled back at the other beam splitter to interfere to generate coherent fringes. Unlike SD-OCT having a CCD to record the whole fringe of the OCT simultaneously, the SS-OCT system applies a balanced photodetector to record the light intensity over time. The swept-source laser is synchronized with the data acquisition to obtain the interference spectrum as a function of time. Therefore, the speed of the OCT system can reach up to several hundred MHz. The typical advantages of SS-OCT compared with SD-OCT are higher imaging depth and higher imaging speed.

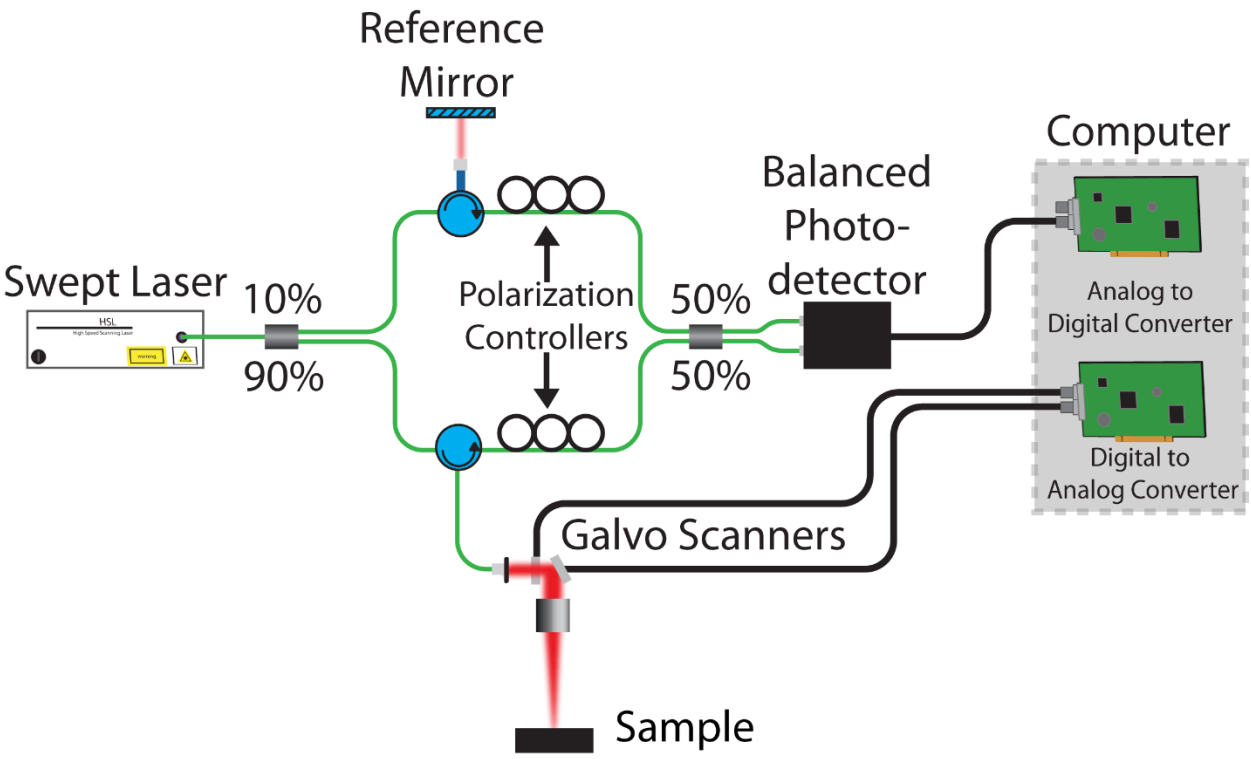

Figure 1.3 Schematic of a typical SS-OCT system

I.5.3 Phase Sensitive OCT (PhS-OCT)

The scale of the axial resolution of OCT intensity signal is micrometer-level. The displacement sensitivity of OCT based on the phase of the OCT signal can reach nanometer scale. Thus, the OCT system with high displacement sensitivity is called phase sensitive OCT (PhS-OCT). In order to increase the displacement sensitivity, the phase stability of the system is critical. Two of the crucial factors of phase stability are the phase stability of the laser source and the stability of the mechanical movable components of the system. Therefore, since TD-OCT needs to move the reference mirror occasionally, its phase stability is less than that of FD-OCT. FD-OCT includes SD-OCT and SS-OCT as described above. In the swept-source laser, there is a sweeping mirror in the laser source to generate the narrow bands of the light by the time to form the light spectrum. In the SD-OCT system,

since the camera can receive the whole bandwidth of the light source at the same time, there is no mechanical movement in the light source. Therefore, the phase stability of SD-OCT is generally better than SS-OCT. In the dissertation, the OCE systems are built based on PhS-OCT.

I.6 Optical Coherence Elastography (OCE)

Optical Coherence Elastography (OCE) is a promising technique to assess tissue elasticity. OCE was first introduced in 1998 by Schmitt et al. OCT was applied to observe the microscale deformation of biological tissue by the compression caused by a piezoelectric actuator [74]. It shows the two-dimensional cross-correlation speckle tracking on the tissue displacement in micrometer-scale. It is also the first *in vivo* OCE application on human skin.

OCE techniques is developed by employing OCT to detect depth-resolved sample deformation to determine tissue biomechanical properties [75, 76]. Researchers can analyze the displacement caused by the excitation and quantitatively apply a suitable mechanical model to measure the tissue's biomechanical properties. As described in Section I.5.3, PhS-OCT can reach nanometer-scale axial displacement sensitivity [77]. Three different types of OCE techniques are applied to quantify biomechanical properties:

1) Compression OCE: compressing the tissue and then observing its local displacement to measure the strain

2) Vibration OCE: observing the harmonic oscillation of the tissue after harmonic excitation

3) Shear wave OCE: elastic wave propagation measurement.

The primary goal of this dissertation is to quantify the biomechanical properties of the lens based on shear wave OCE. I experimented with exciting lenticular tissue and measuring the elastic wave propagation in different lenticular models. An air-puff excitation system is applied to generate the elastic wave propagation on the surface of the lens *ex vivo*. Air-coupled ultrasound transducer and water-coupled ultrasound transducer are introduced in the lenticular biomechanical experiments. Different sources of cataract formation, for example, cataracts induced by low temperature or oxidative environment, are investigated to identify changes in biomechanical properties. Moreover, the elastic wave dispersion in the lenses of different age groups are also measured to estimate the lens viscoelasticity.

I.7 Shear Wave Model

Several viscoelastic models have been applied for elastography investigation, such as the Kelvin-Voigt and the Maxwell models. They have been widely used to model the biomechanical properties of biological tissues [22]. Wave propagation in the tissue can be used to analyze the sample's viscoelastic properties using the previously mentioned models [78]. This has been utilized in ultrasound elastography (USE), magnetic resonance elastography (MRE), and OCE [23].

Based on the structure of the lens, we model the lens as a homogeneous isotropic Kelvin-Voigt body. The wave propagation velocity of the shear wave c can be determined by its shear elasticity and viscosity through the relationship as [79]

$$c(\omega) = \sqrt{\frac{2(\mu_1^2+\omega^2\mu_2^2)}{\rho(\mu_1+\sqrt{\mu_1^2+\omega^2\mu_2^2}}} \tag{1.4}$$

where ρ is the density of the tissue, ω is the frequency of the sample, μ_1 is the shear modulus of the tissue, and μ_2 is the shear viscosity of the tissue, respectively. The effect of shear modulus is much higher than shear viscosity. In this case, μ_2 is negligible and Eq. 1.4 can be simplified to

$$c = \sqrt{\frac{\mu_1}{\rho}}. \tag{1.5}$$

Therefore, the shear modulus and mass density directly determine the shear wave velocity in the tissue. Given the Poisson's ratio ν, the Young's modulus E of the sample can be calculated from its shear modulus as

$$E = 2(1+\nu)\mu_1. \tag{1.6}$$

Since most biological tissues are composed of a high percentage of water, the Poisson's ratio can be estimated as 0.5 [80]. The Young's modulus of the lens tissue can be estimated by shear wave velocity as

$$E = 3\rho c^2. \tag{1.7}$$

Both Eq. 1.6 and 1.7 can be utilized to estimate the elasticity based on the measured shear wave speed.

I.8 Organization of This Dissertation

In this dissertation, OCE is applied to investigate changes in lenticular elasticity during different storage conditions, different types of cataract formations, and lenticular elasticity changes during the aging process based on the shear wave dispersion on the lens.

In Chapter II, the assessments of the effects of the storage medium on the biomechanical properties of the porcine lens were measured with optical coherence elastography. In Chapter III, the biomechanical properties of the lens were measured during cold cataract formation and dissolution. In Chapter IV, the biomechanical properties of the lens were measured during oxidative cataract generation. In Chapter V, the age-related changes in lenticular biomechanical properties were quantified by measuring the dispersion of the shear waves. In Chapter VI, the conclusions of this dissertation are presented with implications for future work.

CHAPTER II – Assessing the Effects of Storage Medium on the Biomechanical Properties of Porcine Lens with Optical Coherence Elastography

In this chapter, I investigated the lenticular biomechanical properties changes caused by the storage medium *ex vivo*. There has been a large amount of research focused on studying the biomechanical properties of the lens *ex vivo*. However, the storage medium of the lenses may affect the biomechanical evaluation during *ex vivo* measurements, which has been demonstrated with other tissues such as the cornea. In this chapter, I utilized a focused micro air-pulse and phase-sensitive optical coherence elastography to quantify the changes in lenticular biomechanical properties when incubated in different media, temperatures, and pHs for up to 24 hours. The results show that the lenses became stiffer when incubated at lower temperatures and higher pHs. Meanwhile, lenses incubated in M-199 were more mechanically stable than lenses incubated in PBS and DMEM.

II.1 Introduction

The changes in viscoelastic properties of the crystalline lens play an important role in the onset and progression of diseases and conditions such as cataract and presbyopia [48, 81]. There has been a large amount of research focused on the biomechanical properties of the lens [66, 82]. However, the storage medium and temperature may affect biomechanical evaluation *ex vivo*, which has been demonstrated with other tissues such as the cornea [83]. The changes in lenticular biomechanical properties can be an important biomarker for lens tissue integrity during lengthy *ex vivo* studies. Here, I performed serial measurements up to 24 hours on extracted porcine lenses with a noninvasive elastography technique, optical coherence elastography (OCE).

In this chapter, OCE was used to measure the changes in lenticular stiffness of excised porcine lenses (N=30) that were stored at various media (PBS, DMEM, and M-199), at various temperatures (4°C, 22°C, and 37°C), and various pHs in M-199 medium. My results show that that lower incubation temperatures or higher pH of medium increase stiffness of the lens.

II.2 Materials and Methods

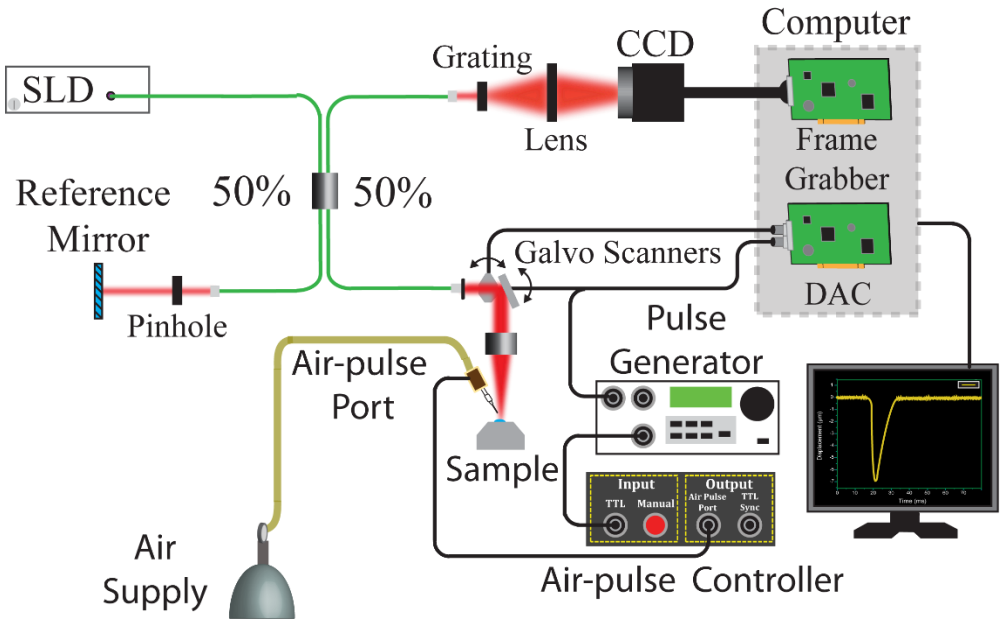

Figure 2.1 Schematic of the experimental setup. CCD – charge-coupled device;DAC – digital to analog converter; SLD – superluminescent diode.

The OCE system was based on a home-built spectral-domain OCT (SD-OCT), an air-pulse excitation system, and a thermal controller for the lenses [84, 85]. A schematic of the system is shown in Fig. 2.1. The SDOCT system utilized a superluminescent diode (SLD) with a central wavelength of 840 nm and bandwidth of 49 nm. The displacement stability of the system was 12 nm in air as measured from the surface of a sample lens. The air-pulse delivery system used an electronically controlled pneumatic solenoid and control unit

to produce a short duration (≤1 ms) air-pulse that was synchronized with the SDOCT system [86]. The air pressure was controlled by a pneumatic valve and monitored by a pressure gauge. The air-pulse was targeted at the apex of the lens. Lenses (n=30) were removed from fresh porcine eye-globes (Sioux-Preme Packing Co. IA, USA). The lenses were separated into three different experiments. The first set of measurements was focused on assessing the effects of the storage medium (PBS, DMEM, and M-199) on lenticular stiffness (N=3 for each medium). The lenses were separated into three groups. Each group was placed into PBS, DMEM, and M-199 medium and incubated for 24 hours at temperature 37°C, and pH=7.0. The effect of incubation temperature on lens stiffness was measured in the second set of experiments. The lenses were separated into three groups and placed into M-199 medium (Sigma-Aldrich Co., MO, USA), incubated for 12 hours in 4°C, 22°C, and 37°C at pH=7.0 (N=3 for each temperature). All measurements were performed at room temperature (22 ^{0}C), when the temperature of the lenses reached room temperature. The effects of pH on the lenticular stiffness were investigated on the third group of lenses. The lenses were separated into four groups and placed in an M-199 medium and incubated for 24 hours at 37°C at pH=4.0, 5.0, 6.0, and 7.0 (N=3 for each pH). During each measurement, the pH value was measured by a pH meter (B10P, VWR International Co., PA, USA). One molar hydrochloric acid solution and NaOH solutions were used to adjust the pH to the target value. The short duration air-pulse induced small amplitude displacements (≤10 μm) on the surface of the lens that propagated as an elastic wave. Successive M-mode images ($n = 251$) were acquired over a ~6.1 mm line [86], where the center of the scan and air-pulse excitation were at the apex of the lens. The group velocity of the elastic wave was determined by the slope of a linear fit of the wave

propagation distances and the corresponding propagation times [87]. The Young's modulus, *E*, was estimated by the surface wave equation [88]

$$E = \frac{2\rho(1+v)^3}{(0.87+1.12v)^2} c_g^2, \tag{2.1}$$

where ρ=1.183g/L was the density [89], v=0.5 was Poisson's ratio [6], and c_g was the OCE-measured elastic wave group velocity.

II.3 Results

Figure 2.2 shows the results of Young's modulus estimations for the lenses after storage in different media. The estimated Young's modulus of the lenses that were incubated in PBS showed a significant increase over 18 hours, and it increased from 7.3±0.7 kPa to 13.0±0.3 kPa. However, there was a slight decrease in lenticular stiffness after 24 hours of incubation as compared to 18 hours of incubation in PBS. After 12 hours, the lenses incubated in DMEM showed an increase in stiffness from 6.1±0.6 kPa to 8.3±0.2 kPa. However, there was a dramatic increase in stiffness from 6.1±0.6 kPa at 0 hours to 13.7±1.8 kPa and 11.6±2.9 kPa after 18 and 24 hours of incubation, respectively. However, the lenses incubated in M-199 showed a decrease in stiffness over the 24-hour incubation period (from 8.3±0.6 kPa at 0 hours to 7.0 ± 0.6 kPa at 24 hours). These results indicate that the M-199 medium preserves the biomechanical properties of excised porcine lenses better than DMEM or PBS at 37°C over a period of 24 hours.

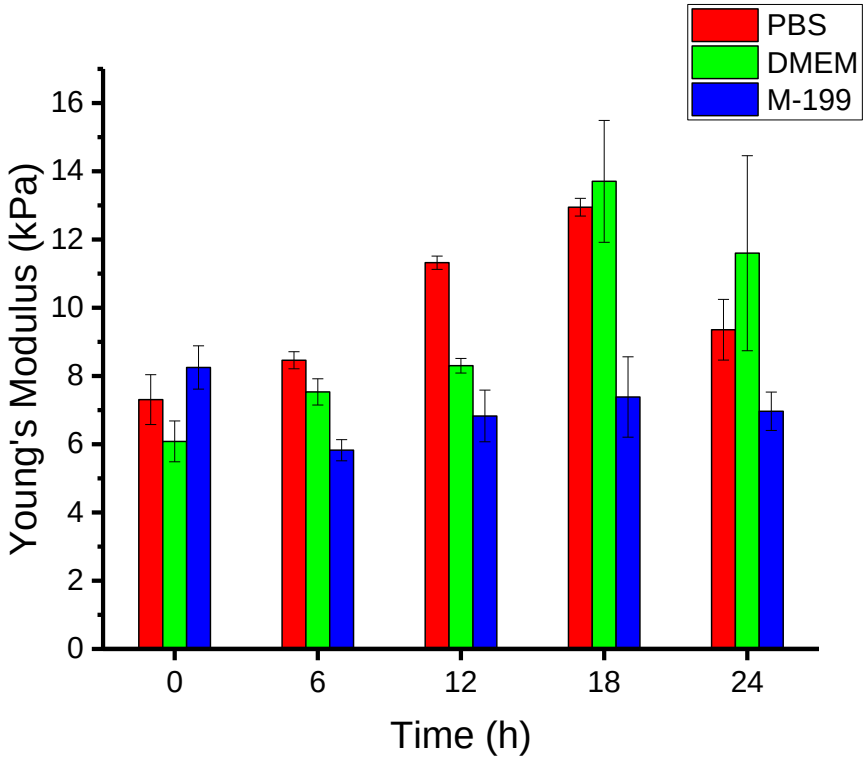

Figure 2.2. The estimated Young's modulus of the lenses incubated in the different indicated media over 24 hours (N=3 for each medium).

As Fig. 2.3 shows, Young's modulus of the lenses that were incubated at 4°C, 22°C, and 37°C. The stiffness of the lenses incubated at 4°C increased from 6.3±0.4 kPa to 7.0±0.2 kPa after 12 hours. The Young's modulus of the lenses incubated at 22°C increased from 6.0±0.4 kPa to 6.8±0.4 kPa after 12 hours. After 12 hours, Young's modulus of the lenses incubated at 37°C decreased from 5.5±0.2 kPa to 4.4±0.4 kPa. The results showed that while the stiffness of the lenses increased when incubated for 12 hours at 4°C and 22°C, the lenticular stiffness decreased slightly when the lenses were incubated for 12 hours at 37°C.

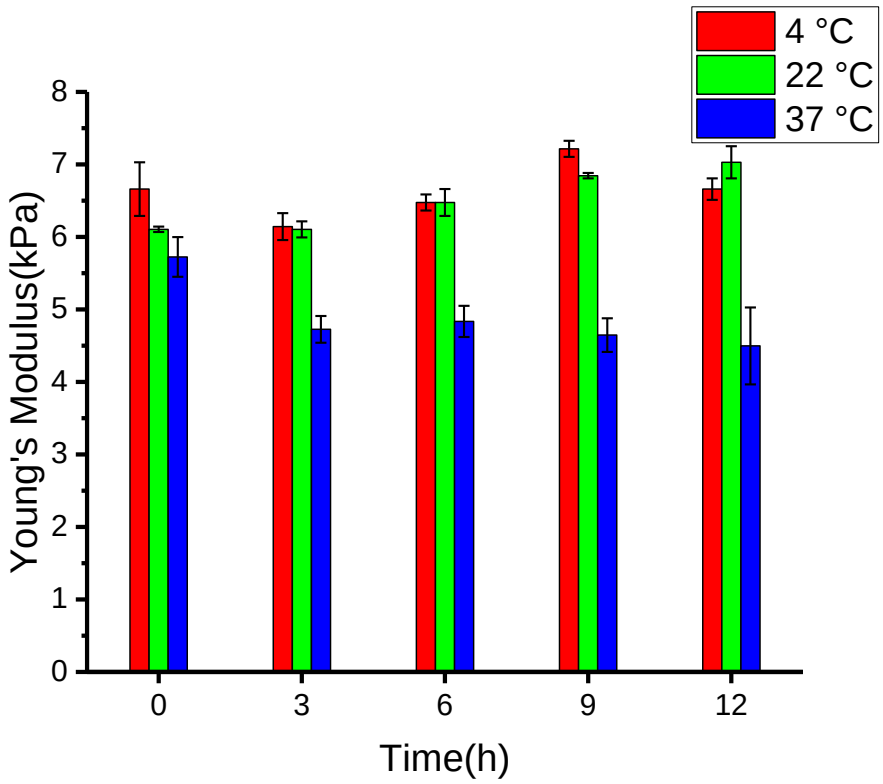

Figure 2.3. The estimated Young's modulus of the lenses incubated in M-199 medium at 4°C, 22°C, and 37°C over 12 hours (N=3 for each temperature).

Figure 2.4 plots the results of the estimated Young's modulus of the porcine lenses incubated in M-199 medium at different pHs (4.0, 5.0, 6.0 and 7.0). The Young's modulus of the lens in pH=7.0 medium decreased slightly from 7.4±0.8 kPa to 5.7±1.5 kPa. However, as the pH value decreased, the stiffness of the lenses increased, indicating damage to the lenses. The most dramatic change in elasticity occurred when the lenses were stored at a pH of 4.0, where the stiffness increased from 7.1±0.3 kPa at 0 hours to 12.0±1.3 kPa after 12 hours.

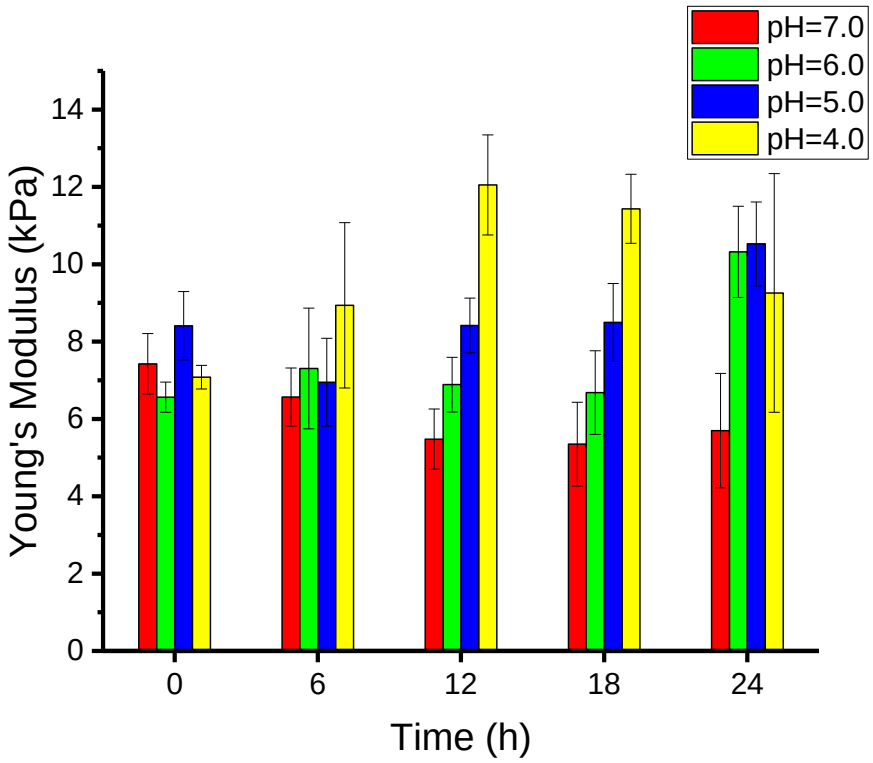

Figure 2.4. The estimated Young's modulus of the lenses incubated in M-199 media at various pHs over 24 hours (N=3 for each pH).

II.4 Discussion

Different culture media have different ingredients for biological tissues. It is understandable that the closer the medium compared with normal biological fluid, the better the medium is for the biological tissues.

Most of the enzymes have their suitable temperature and the structural proteins have the temperature for their biological activities. Low temperature can make the enzymes and structural proteins change their biological activities to change the biomechanical properties. High temperature may make the enzymes and structural proteins denature and lose their biological activities to change the biomechanical properties. In this chapter, I did

not measure the effect of high temperature. Future work needs to be done to measure the high temperature effect.

pH value has similar effects on the biological tissues compared with temperature on enzymes. However, low or high pH values can both denature the enzymes and structural proteins. In this chapter, only low pH value was measured, while high pH value was not considered. Therefore, high pH value measurement is necessary in the future work.

In this chapter, I evaluated the changes of *ex vivo* porcine lenticular biomechanical properties after they were incubated in different media, temperatures, and pHs for up to 24 hours. The results showed that OCE could be used to assess lenticular biomechanical properties and might be useful for detecting and, potentially, characterizing lenticular integrity.

II.5 Conclusion and Future Work

M-199 medium, generally used to culture fibroblasts, preserved the stiffness of the lenses up to 24 hours better than PBS or DMEM. The lenses incubated at 37 °C showed a decrease in elasticity, but the lenses incubated at 4°C and 22°C showed an increase in stiffness, indicating possible structural changes in the lens. The more acidic the storage medium was, the stiffer the lenses became after 12 to 24 hours, indicating that the acidic media caused structural damage to the lenses. My future work will entail utilizing a more robust analytical model to obtain quantitative biomechanical parameters such as viscoelasticity as well as evaluating the effects of lenticular biomechanical properties while the lens is within the eye-globe, which is stated in Chapter V.

CHAPTER III – Optical Coherence Elastography of Cold Cataract in Porcine Lens

In this chapter, I discussed a kind of reversible cataract – cold cataract. Cataract is one of the most prevalent causes of blindness around the world. Understanding the mechanisms of cataract development and progression is important for clinical diagnosis and treatment. Cold cataract has proven to be a robust model for cataract formation that can be easily controlled in the laboratory. There is evidence that the biomechanical properties of the lens can be significantly changed by cataract [81]. Therefore, early detection of cataract, as well as evaluation of therapies, could be guided by characterization of lenticular biomechanical properties. In this chapter, I utilized optical coherence elastography (OCE) to monitor the changes in biomechanical properties of *ex vivo* porcine lenses during formation of cold cataract. Elastic waves were induced in the porcine lenses by a focused micro air-pulse while the lenses were cooled, and the elastic wave velocity was translated to Young's modulus of the lens. The results show an increase in the stiffness of the lens due to formation of the cold cataract (from 11.3 ± 3.4 kPa to 21.8 ± 7.8 kPa). These results show a relation between lens opacity and stiffness and demonstrate that OCE can assess lenticular biomechanical properties and may be useful for detecting and potentially characterizing cataracts.

III.1 Introduction

Cataract is clouding of the crystalline lens that can severely impair vision with faded colors, blurry vision, halos around light, and poor night vision. Approximately 1/3 of all people with some form of vision impairment have cataract [90]. Eventually, over 1/2 of patients with cataract undergo vision loss [90]. There are numerous causes of cataract, such

as aging, trauma, diabetes, obesity, congenital genetic deficiencies, and environmental exposure to toxins [91]. Usually, cataract is progressive and requires surgical interventions for treatment. The specific underlying mechanism of cataract formation is still unknown, but there are reports that the stiffness of the cataract lenses in human is significantly higher than that of normal lenses [81].

One of the simplest models to investigate cataract formation is a cold cataract. Cold cataract is a reversible opacification induced in the nucleus of lenses by lowering the temperature [92, 93]. This phenomenon enables me to study a controlled opacification and to investigate the physicochemical processes associated with a reversible form of cataract. It has been shown that the precipitation of γ-crystallin is correlated with cold cataract development in the lens [94]. Gamma crystallin is one of the predominant crystallins in the lens nucleus that is responsible for optical transparency [92]. This reversible opacification is a result of a phase separation of the cytoplasmic proteins into coexisting protein-rich and protein-poor liquid domains. Zigman et al. demonstrated that γ-crystallin is the major component of both fractions [93]. Gamma crystallin has been shown to be the only one of the three soluble protein fractions capable of acting as a cryoprotein. The relative concentration of γ-crystallin as compared with the amounts of α- or β-crystallin in solution determines whether cold precipitation occurs. Therefore, since the nucleus of the lens contains more γ-crystallin than the cortex, opacification predominantly occurs in the lens nucleus [92]. Moreover, the concentration of γ-crystallin can also affect the appearance of cold cataract [94]. Previous research has been focused on biomolecular and biochemical changes during cold cataract formation [95-97]. For example, the formation of cold cataract has been observed in lenses of various animals, such as fish and cattle, and the contribution

of different types of crystallins was evaluated [96, 97]. Moreover, the optical characteristics of lenses with cold cataract were assessed [95, 98]. Despite this research, there is a lack of work focused on the biomechanical effects of cold cataract on the lens.

Mechanical testing is commonly used to evaluate the biomechanics of ocular tissue including the lens, however, such technique is invasive and destructive, which limits its clinical applicability [99, 100]. Several non-destructive techniques have been proposed to evaluate lenticular biomechanical properties [101-103], including acoustic-based elastographic techniques [101, 104-106]. While these techniques have revealed critical information, they lack spatial resolution and sufficient contrast. Thus, OCE was applied for this research.

In the previous work of my lab, they have used dynamic OCE and acoustic-based methods for noninvasively assessing lenticular biomechanical properties [8, 64, 66, 82, 107]. They have demonstrated that the biomechanical properties of the crystalline lens can be measured *in situ* and quantified variations in the stiffness of mammalian lenses as a function of age and intraocular pressure [64, 66, 107].

In this chapter, I induced cold cataracts in *ex vivo* porcine lenses, and assessed the lenticular stiffness with elastic wave-based OCE. After OCE measurements of the fresh lenses during temperature decrease, the cold cataract was induced by lowering the temperature of the isolated crystalline lenses for 6 hours. Then, the OCE measurements were repeated as the temperature was increased. After the cataract formation the lenses showed an increase in elastic wave velocity in comparison with fresh lenses. The difference in wave velocity between cataract and fresh lenses disappeared after the cataract dissolved.

The results indicate the stiffness of the lens has the correlation with lens opacity in a cold cataract model.

III.2 Materials and Methods

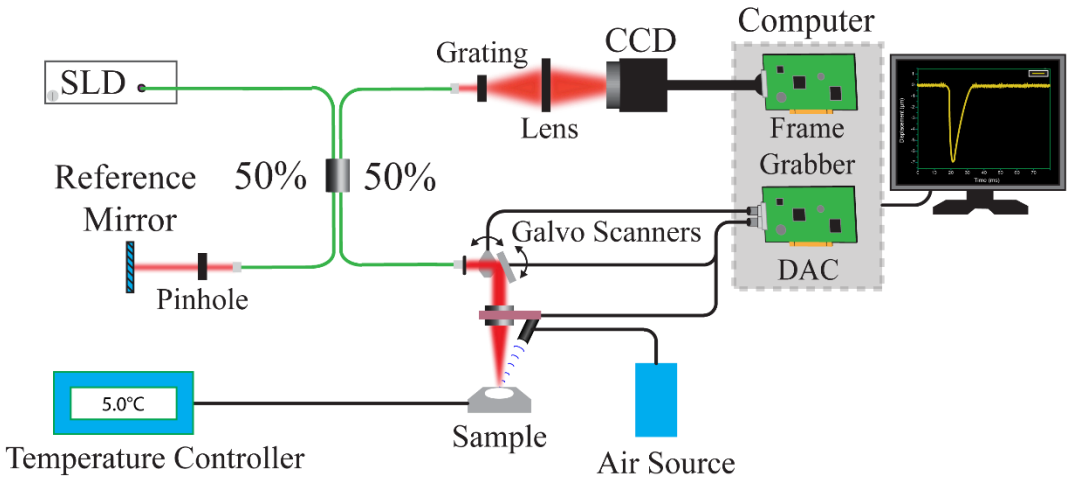

Figure 3.1. Schematic of the experimental setup during the OCE measurements.

The OCE system was based on a home-built spectral domain OCT (SD-OCT) system and an air-pulse excitation system, as shown in Fig. 3.1 [108, 109]. The SD-OCT system utilized a superluminescent diode (SLD) light source with a central wavelength of 840 nm, bandwidth of 49 nm, and output power of 18 mW. The acquisition speed of camera was set as 25 kHz. The displacement sensitivity of the OCE system was measured as 12 nm in air. The air-pulse delivery system used an electronically controlled pneumatic solenoid and control unit to produce a short duration air-pulse (<1 ms) that was synchronized with the SD-OCT system frame trigger [86]. To image deep inside the lens and visualize the formation of the cold cataract, I utilized a commercial swept source OCT (SS-OCT) system (OCS1310V2, Thorlabs Inc., NJ, USA) with a central wavelength of 1300 nm, bandwidth of ~100 nm, and sweep rate of 200 kHz [110].

Preliminary measurements were performed on tissue-mimicking agar phantoms (1%, w/w, Difco Nutrient Agar from BD, Franklin Lakes, NJ) and gelatin phantoms (3%, w/w, Type A gelatin, 250 Bloom/8 Mesh, PB Gelatins/PB Leiner, Davenport, IA). The phantoms were cast by standard methods as described in the previous work of my lab [109, 111]. Cylindrical culture dishes with inner diameter of 50 mm and height of 12 mm were used to mold the phantom samples. After that, the samples were placed into the refrigerator at ~4°C [111]. The phantoms were measured by OCE as the phantoms warmed (N=3 for both gelatin and agar phantoms). The phantom temperature was controlled by the system consisting of a holder and a thermoelectric cooler that was used also to control the temperature of the lenses shown in Fig. 3.1. In addition, the temperature on the phantom surface was monitored by a noncontact infrared thermometer (CF-IR, ThermoWorks, UT).

Seven whole porcine eyes from animals within 4-6 months of age were shipped overnight on ice (Sioux-Preme Packing Co., IA, USA). The freshly extracted lenses were placed in the custom apparatus of the temperature controlling system. The lenses were half submerged in 1X PBS when OCE measurements were not being performed. Additional 1X PBS was topically dropped on to the upper surface of the lenses every 20 seconds to make sure the lenses were hydrated. Measurements of the fresh lenses were taken at 3 °C intervals from 21 °C to 6 °C. It required approximately 5 minutes to reach the 3 °C temperature increase for every step. Once the target temperature was reached, I waited for 2 minutes to make sure the temperature of the thermoelectric cooler was the same as that of the noncontact thermometer. After the initial measurements on the fresh lenses, the lenses were put into a 4 °C refrigerator for 6 hours, also submerged in 1X PBS, to induce a cold cataract. Cold cataract was identified by visual inspection and confirmed by SS-

OCT imaging. The lenses were removed from the refrigerator, placed in a holder, and the OCT imaging and OCE measurements were repeated for the chilled lenses while temperature was increased from 6 °C to 21 °C, also at 3 °C increments with the same measurement interval.

To evaluate the temperature distribution inside the samples, separate experiments were performed on a 1% agar phantom and porcine lens. The samples were partially immersed in the PBS solution as with the previous measurements. A thermocouple (Omega Engineering Inc., Norwalk, CT) with a diameter of 0.1 mm was used to probe the temperature gradient inside the samples at 4 equally spaced positions along the entire depth of the sample 2 minutes after the temperature reading from the temperature control system was stable. One agar phantom, two normal lenses, and two cataract lenses were used in these experiments.

OCE measurements were performed by inducing small amplitude displacements (≤10 μm) using a short duration air-pulse (≤1 ms) on the surface of the lenses and phantoms. M-B-mode imaging was performed, where the OCT probe beam was held stationary at a given position, and an air-pulse was excited by the air-pulse system. Then, the OCT probe beam was moved to the next position and another elastic wave was excited. By synchronizing the OCT system frame trigger with the air-pulse control unit, I effectively imaged the same elastic wave at a frame rate equal to the OCT system A-scan rate (i.e., camera speed) [86]. Successive M-mode images (n=251) were acquired by the SD-OCT system over a ~6.1 mm line, where the center of the scan and air-pulse excitation were at the apex of the lens. The scan time for one position was approximately 10 ms, and the entire M-B scan time

was approximately 30 s. The air-pulse induced a low-amplitude displacement at the apex of the lens, which then propagated transversely as an elastic wave. The raw temporal phase profiles were unwrapped and then converted to displacement after correcting for the refractive index mismatch and surface motion [112]. The displacement profiles along the propagation path (i.e., along the curvature of the sample) were then processed by a cross-correlation algorithm to obtain the elastic wave propagation delays. In short, the displacement profile at the excitation was used as a reference profile, and the displacement profiles from successively more distant positions were then cross-correlated with the reference profile. The peak of the subsequent cross-correlation was selected as the temporal delay for the elastic wave propagation to that OCE measurement position. A linear fit was then performed on the elastic wave propagation delays and their corresponding distances (incorporating the curvature of the sample). I selected the ~3 mm central part of the lens for the group velocity estimation to make sure that the measured group velocity was over cold cataract. The speed of the elastic wave was converted to the Young's modulus value by the surface wave equation Eq. 2.1. Before testing, all porcine lenses were physically measured, and there were no detectable changes in sample geometry.

III.3 Results

Figure 3.2 shows the OCE-measured group velocities for agar and gelatin phantoms as a function of temperature. As seen in Fig. 3.2, gelatin and agar gels demonstrate different levels of dependence of the elastic wave speed on temperature. While the group velocity in the gelatin phantom decreased from ~1.9 m/s to ~1.7 m/s as the temperature increased from 5 °C to 20 °C, the velocity in the agar phantom did not show significant changes with temperature, decreasing from 2.2 m/s to 2.1 m/s. Statistical testing by a one-way ANOVA

showed that there was statistical significance of samples on the stiffness of the 3% gelatin phantoms (F (2, 0.95) = 5.00, p=0.03) but no statistical significance of samples on the stiffness of the 1% agar phantoms (F (2, 0.95) = 2.46, p=0.14) as a function of temperature. Additional measurements of the temperature gradient in the agar phantom demonstrated a monotonic dependence of the temperature with depth, such that the maximum difference between the top of the phantom exposed to air and PBS solution was 1.5 °C. The mean difference between the temperature inside the phantom and PBS solution was 0.55 °C with a standard deviation of 0.56 °C.

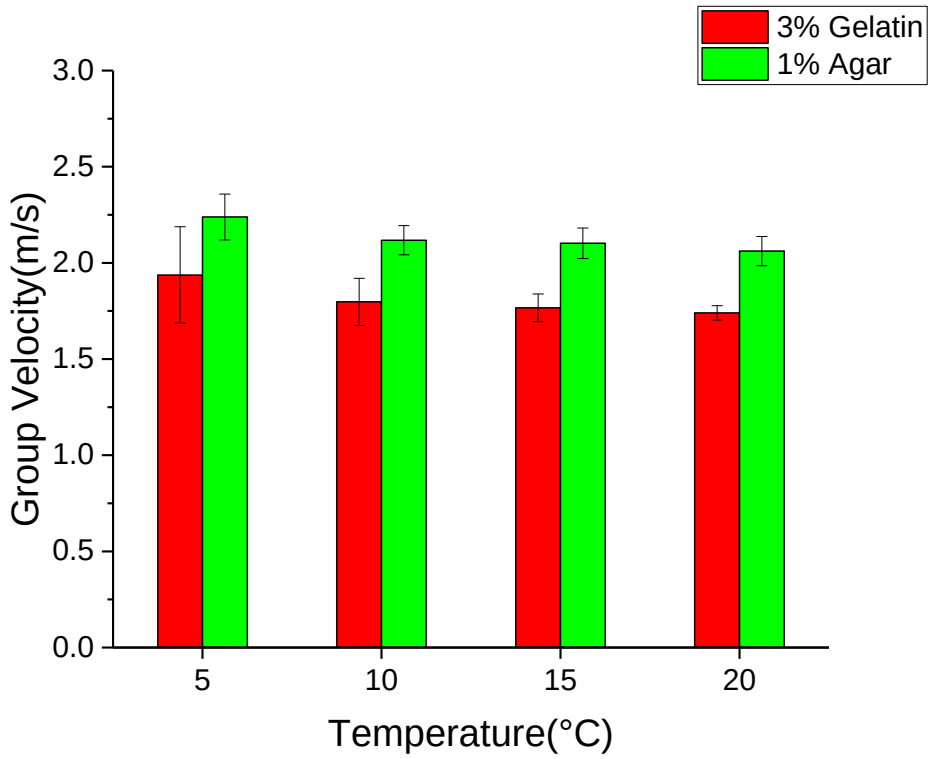

Figure 3.2. The OCE-measured group velocity in a 3% gelatin and 1% agar phantoms as a function of temperature.

Figure 3.3 shows images taken by a standard dissecting microscope (Stemi 508, Carl Zeiss Microscopy, LLC, Thornwood, NY, USA) while (a) chilling the fresh lens from 21

°C to 6 °C and (b) warming the lens from 6 °C to 21 °C after being placed in a 4 °C refrigerator for 6 hours. As seen in Fig. 3.3(a), the fresh lens was clear, and there was no apparent change in the lens transparency while the lens was cooled. However, after 6 hours at 4 °C, there is a clear opaque region in the center of the lens, which then disappeared as the lens was warmed to 21 °C.

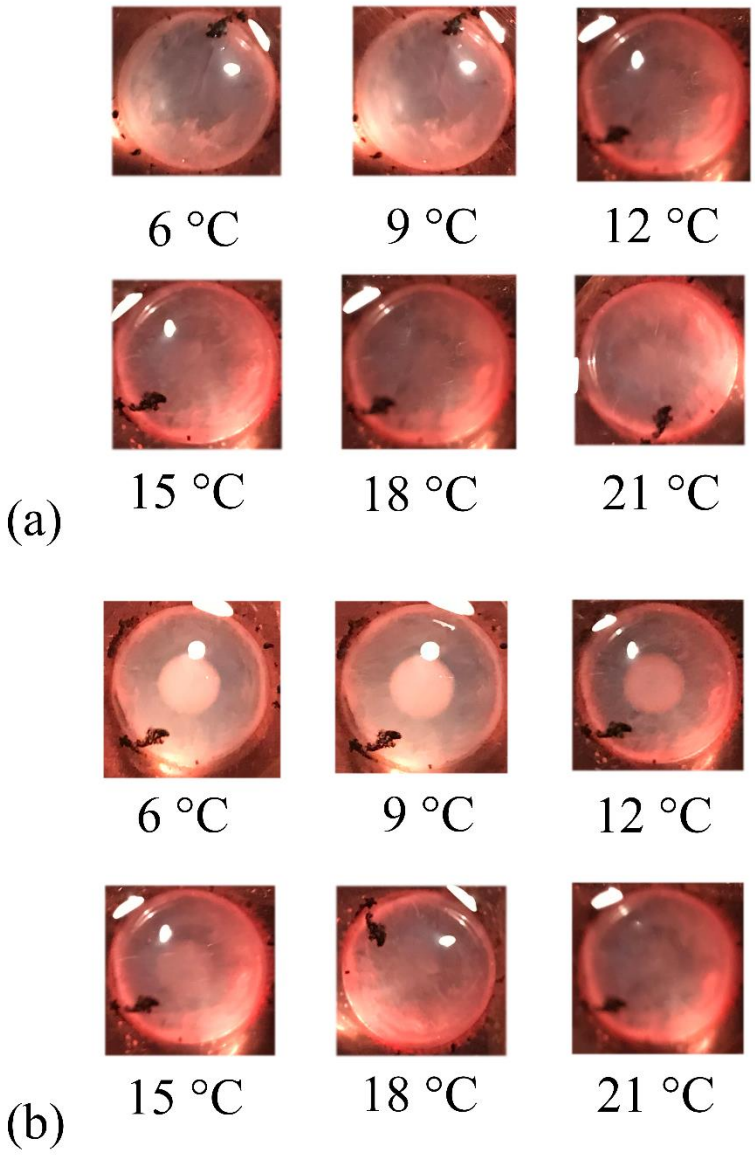

Figure 3.3. (a) Images from a dissecting microscope while a fresh porcine lens was (a) cooled from 21 °C to 6 °C and (b) warmed from 6 °C to 21 °C after being in a 4 °C refrigerator for 6 hours.

The OCT images corroborate these results. Figure 3.4 shows the OCT images of the lens before and after the formation of cold cataract. The OCT images of fresh lens did not show any scattering differences as a function of temperature while it was cooled. However, there was more scattering and a clear formation of aggregated scattering structures within the

lens after cold cataract was formed. When the temperature was increased, the aggregated scattering structure shrank until it disappeared when the temperature increased beyond 12 °C.

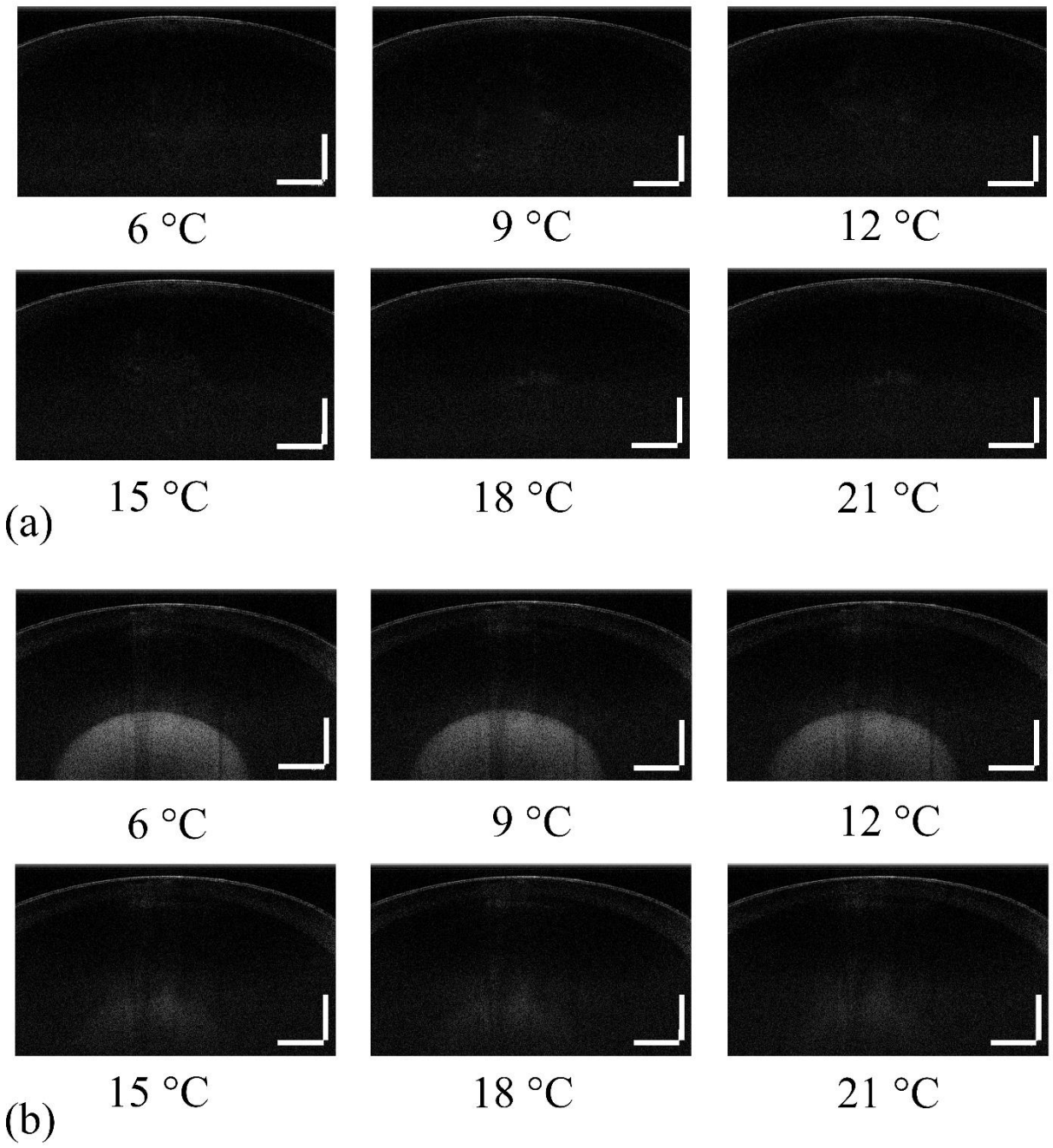

Figure 3.4. (a) OCT structural images of a fresh porcine lens that was (a) cooled from 21 °C to 6 °C and (b) warmed from 6 °C to 21 °C after being in a 4 °C refrigerator for 6 hours. The scale bars are 1 mm.

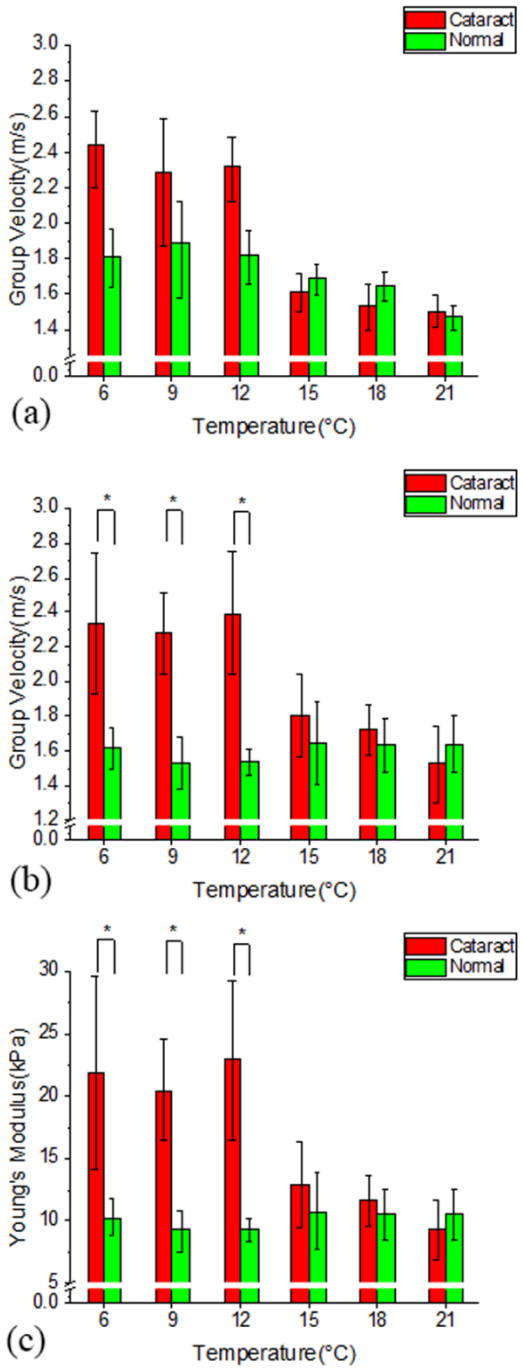

Figure 3.5. The measured group velocities and estimated Young's moduli for the fresh lenses and lenses with induced cold cataracts.

The relationship between stiffness and temperature before and after the cataract was formed is shown in Fig. 3.5. Figure 3.5(a) shows the elastic wave group velocity for one

representative sample with and without cataract in the temperature range from 6 °C to 21 °C. The error bars represent the error estimated by the 95% confidence interval for the slope of a linear fit of thepropagation time versis distance. Figure 3.5(b) illustrates the averaged elastic wave group velocities for all 7 samples as a function of temperature. Figure 3.5(c) shows the calculated Young's moduli for all 7 samples. For Figure 3.5(b) and (c), the error bars are the inter-sample standard deviation. The asterisks indicate statistical significance ($p<0.05$) determined by Student's t-test. As seen in Figs. 3.3 and 3.4, the cataract began to disappear as the lens was warmed beyond 12 °C. The group velocities in the samples that were cooled for 6 hours at 4 °C (cataract) decreased as they were warmed. Statistical testing by one-way ANOVA showed that there was no statistically significant difference of the group velocities for different temperatures in both cataract and normal groups ($F(5, 0.95) = 0.69$, $p=0.64$). A t-test showed that the difference in stiffness between cataract samples and normal samples was significant ($p = 0.003$). Based on this result, I performed further pair-wise t-tests (with Bonferroni correction for multiple testing) for each temperature, which showed a significant difference between the stiffness of the cataract and normal lenses at 6, 9, and 12°C ($p = 0.012$, 0.007, and 0.0015, respectively). The values of Young's modulus of the lenses shown in Fig. 3.5(c) were calculated using Eq. 2.1. The mean value of the estimated Young's moduli of cataract lenses for 6, 9, 12 °C was 21.8 ± 7.7 kPa, while the mean value of the Young's moduli of the normal lenses at this temperature was 9.6 ± 1.4 kPa. For 15, 18, and 21 °C, the cataract groups have the mean value of the Young's modulus of about 11.3 ± 3.4 kPa, and while the normal lenses groups have the mean value of the Young's moduli of 10.6 ± 2.3 kPa.

The measurements of the internal temperature gradient in cataract and normal lenses showed results similar to the results for the agar phantom, with no significant difference between normal and cataract lenses, within the measured temperatures range. For the normal lens the mean difference between the internal temperature of the lens and the temperature of PBS solution was 0.43 ± 0.38 °C, while for cataract lens, it was 0.42 ± 0.34 °C. The maximum differences were 1.1 °C and 1.0 °C for normal and cataract lenses, respectively.

III.4 Discussion

While the relationship between the stiffness of the lens and the age is well known [32, 66, 81, 106], the influence of cataract formation on the lens stiffness is still unclear. In this chapter, I have demonstrated that in a porcine cold cataract model, the stiffness of the lens has a correlation with opacity of the nucleus. The speed of the elastic wave (i.e., stiffness of the lens) significantly decreased when cataract dissolved between 12 °C and 15 °C. Similar to the optical properties, the changes in lens stiffness are reversible, and possibly connected with the precipitation of γ-crystallin. Because the changes in lens opacity are localized in the nucleus, I could assume that the changes in lens elasticity are also localized in the nucleus, as it has been shown that there is an elastic gradient in the lens [101, 106]. Although the OCE measurements were performed only on the lens surface, it is known that the surface wave is also sensitive to deep layers of the medium, depending on the wavelength of the elastic wave [113-115]. Though the scan width was greater than the width of the cold cataract, the width that I used to calculate group velocity was only ~3 mm across the center of the apex of the lens, which means the group velocity measurements were from the region over the cataract. In this case, as seen in Fig. 3.4, the cataract was

located 2~3 mm below the surface of the lens. However, the frequency content of the elastic wave was below 1 kHz (centered around ~550 Hz). With a speed of ~1.8 m/s, the corresponding elastic wave wavelength was ~3.3 mm. Therefore, the estimated Young's modulus reflects some spatially averaged elastic modulus, including part of the nucleus, but likely underestimates the nucleus stiffness. Additional studies are required to better understand the spatial elasticity distribution in cataract lenses, and my future studies will be focused on a much wider range of elastic wave frequencies to probe the elasticity gradient of the lens.

Previous research shows that the threshold of the cold cataract might vary in different species [95-97]. Zigman et al. [93] demonstrated that the optical density of the mouse lens is stable up to 11 °C. In my experiments on porcine lenses, the threshold was between 12 °C and 15 °C. The percentage of γ-crystallin in porcine nucleus is about 30% [116], while the mouse nucleus contains 60% γ-crystallin [117]. The fish lens has 30.5% γ-crystallin, and the cataract temperature threshold was demonstrated to be about 5 °C [97, 118]. The relationship between γ-crystallin and cold cataract threshold needs to be further elucidated and is an avenue of future research. Although many biological tissues demonstrate the dependence of elasticity on temperature [119-122], similar to the temperature dependence for gelatin phantoms shown in Fig. 3.2, I did not observe a significant change of the wave speed (i.e., stiffness) with temperature in fresh lenses (Fig. 3.5). Also, the cataract lenses were slightly softer than fresh lenses at 21 °C as seen in Fig. 3.5. This observation can be associated with residual effect of cataract formation, or overall changes in lens elasticity after 6 hours of storage, for example, the loss of crystalline proteins after the storage [53]. Previous work has shown that the duration of heating can also increase the elasticity of the

lens [119]. When human lenses were heated for 4 hours, the shear modulus was ~4 kPa. When the heating time was increased to 8 hours, the shear modulus increased to about ~7 kPa because of proteins denaturing at 50 °C. In contrast, freezing porcine lenses at -80 °C caused a decrease in the shear modulus from ~0.9 kPa to ~0.3 kPa after 4 weeks. Nevertheless, there is little or no research focused on the changes in lenticular biomechanical properties due to moderately temperatures (near 4 °C). I postulate that the aggregation of γ-crystallins formed during cold cataract contributes to an increase in lenticular stiffness. Further analysis is needed to confirm or disprove this hypothesis and is the focus of future work.

Although the difference in the spatial distribution of temperature in the lens could be a possible reason for the difference in stiffness between cataract and normal lenses, my measurements show that the temperature gradient in the normal and cataract lenses are similar, such that it is unlikely that the temperature distribution can be a reason for the difference in the elastic wave velocity. The temperature gradient in the agar phantom was greater but can be explained by the different thermal conductivity and the size of the agar phantom.

The values of Young's modulus obtained based on Eq. 2.1 are in agreement with literature data for porcine lenses [100, 123]. However, the distribution of elasticity in crystalline lens is inhomogeneous [32, 105]. In addition, viscous properties also could play a significant role in the process of surface wave propagation [99, 105, 106]. Therefore, application of Eq. 2.1 obtained for an elastic, homogeneous half-space has significant limitations. More sophisticated analytical and computational models are needed to provide

more accurate values of lens viscoelasticity, which I am focused on developing. The tentative research about lenticular viscoelasticity is stated in Chapter V.

III.5 Conclusion

In this chapter, I evaluated the changes in the biomechanical properties of porcine lenses *ex vivo* during the formation of cold cataract using OCE. The lenses with cold-induced cataracts showed an increase in elastic wave velocity, and correspondingly, stiffness, in comparison with fresh lenses. However, the difference in stiffness between cataract and fresh lenses disappeared after the cataract dissolved. These results show that OCE can assess lenticular biomechanical properties and may be useful for cataract characterization.

CHAPTER IV – Elasticity changes in the crystalline lens during oxidative damage and the antioxidant effect of alpha-lipoic acid measured by optical coherence elastography

In this chapter, I pushed my investigation forward on the age-related cataracts. Understanding the mechanisms of cataract development and progression is essential to enable early clinical diagnosis and treatment to preserve visual acuity. Reductive chemicals are potential medicines effective on cataract treatment. In this chapter, I investigated the cataract-induced oxidative damage in the crystalline lens and a kind of reductant, α-lipoic acid (ALA), ability to reduce the damage. I created oxidative environment to investigate the relationship between the progression of oxidative permanent cataract and lenticular biomechanical properties measured by dynamic optical coherence elastography in porcine crystalline lenses *ex vivo*. The efficacy of ALA to minimize the stiffening of the lens was also quantified. The results showed a significant increase in Young's modulus of the lens due to the formation of the oxidative cataract. I found a statistically significant difference between Young's modulus of the lenses stored in phosphate-buffered saline and ALA solution after incubation in H_2O_2 solution for 3 hours (43.0± 9.0 kPa versus 20.7± 3.5 kPa, respectively). These results show that the lens stiffness increases during oxidative cataract formation, and ALA has the potential to reverse stiffening of the lens caused by oxidative damage.

IV.1 Introduction

Oxidative stress is often considered a major factor contributing to lens changes during aging and cataract formation [124-130]. The oxidation of methionine residues and loss of sulfhydryl groups of proteins are both progressive as the cataract worsens until 90% of

cysteine and half the methionine residues are oxidized in the most advanced form of cataract [35, 130, 131].

Glutathione (GSH) in the crystalline lens functions as an antioxidant for lens proteins, and loss of nuclear GSH may be the critical event that precedes age-related cataract formation [9, 130, 132-134]. Previous studies have indicated an important hydroxyl radical scavenging function of GSH in lens epithelial cells to preserve the lens by offering a reductive environment [135, 136]. Therefore, antioxidants may have the potential to protect the lens from oxidative damage and, subsequently, cataracts. Several antioxidants have been reported to delay cataract formation in ex vivo and in vivo animal models [91, 132, 137]. In the past few decades, α-lipoic acid (ALA) has emerged as an antioxidant and nutritional supplement [138] that, among other benefits, has been shown to be effective in preventing the onset and progression of cataract [139-144]. Moreover, it has recently been demonstrated that alpha-lipoic acid has a potential therapeutic role in restoring accommodation to the presbyopic eyes by reducing lens stiffness [9]. Previous research shows that both presbyopic [32, 99, 100] and cataract [81] lenses are stiffer than healthy lenses, which suggests that monitoring the biomechanical properties of the lens can provide important information about the mechanisms of lens aging, presbyopia, and cataract formation. Furthermore, it has been hypothesized that progressive age-dependent hardening of the crystalline lens may be responsible for both presbyopia and age-related cataracts [127].

In the previous work of my lab, they demonstrated that the biomechanical properties of the lens could be measured *in situ* and that the lenticular biomechanical properties could be quantified as a function of age and intraocular pressure by using dynamic OCE [64, 66,

145]. In Chapter III, I used shear wave OCE to show the correlation between lens opacity and elasticity during cold cataract formation in a porcine model *ex vivo* [36].

To simulate cataract formation, I incubated the lenses in hydrogen peroxide. It has been shown that there is a close parallel between protein modifications found in cataract and those generated with hydrogen peroxide [146]. In this chapter, I first applied OCE to observe the elasticity of the lens during the oxidation process of the lenses. Then I investigated the changes in the lens elastic properties during oxidative cataract formation and the effect of ALA on resisting oxidation and lens hardening. I used shear wave OCE to quantitatively evaluate the changes in surface wave velocity and Young's modulus during cataract formation. After measuring surface wave propagation in fresh porcine lenses, the lenses were incubated with hydrogen peroxide (H_2O_2) to induce oxidative cataracts [142]. Subsequently, the lenses were incubated in ALA to investigate their effect on cataract development. The results show a significant increase in lens stiffness during cataract formation and the potential of ALA to reduce the stiffening of the lens caused by oxidative damage.

IV.2 Materials and Methods

IV.2.1 Experimental Set-up

The dynamic OCE system is built based on a phase-sensitive spectral domain OCT (SD-OCT) system, which is combined with an air-pulse excitation system. A schematic of the experimental system is shown in Figure 4.1 and has been described in the previous work of our lab [108, 109]. The OCE system includes a superluminescent diode (SLD, S840-B-I-20, Superlum Co., Cork, Ireland) with a central wavelength of 840 nm and a bandwidth of 49 nm. The acquisition speed of the camera (spL4096-140km, Basler AG, Ahrensburg,

Germany) was set as 40 kHz. The displacement stability of the system was measured as 12 nm in air. The air-pulse excitation system used an electronically controlled pneumatic solenoid and control unit to produce a short air-pulse (≤1 ms) [109]. The pressure was controlled by a pneumatic valve and monitored by a pressure gauge. The air-pulse was synchronized with the SD-OCT system frame trigger [86].

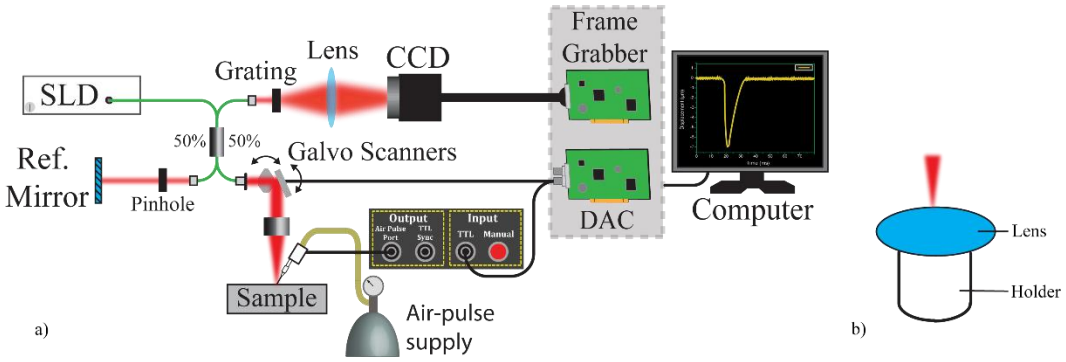

Figure 4.1. The Schematic of the OCE system. (a) A micro-air pulse is co-aligned with an SD-OCT system to detect air pulse-induced elastic waves on the surface of the excised porcine lens and (b) the sample holder.

IV.2.2 Sample Preparation

Fifteen porcine eyes from animals within 4-6 months of age were shipped overnight on ice (Sioux-Preme Packing Co., Sioux City, IA, USA). The lenses were extracted carefully from the eye globes and visually inspected to ensure there was no damage. The lenses were divided into five groups of three lenses each and incubated at 37 °C in different storage media. The first group was incubated in a solution of 500 mM H_2O_2 in 1X phosphate buffered saline (PBS) for 9 hours. The second group was first incubated in the peroxide solution for 3 hours and then was removed and incubated in a 100 mM ALA (sodium salt) solution for an additional 6 hours (H_2O_2 → α-Lipoic Acid). The third group was incubated

in the H_2O_2 solution for 3 hours and then was removed and incubated in 1X PBS for 6 hours (H_2O_2 →PBS). The fourth group was incubated in the ALA solution for 9 hours. Finally, the fifth group was incubated in 1X PBS for 9 hours. The OCE measurements of lens elasticity were repeated every 3 hours for 9 hours.

PBS-only group was the negative control. ALA-only group was a negative control to investigate if ALA would cause changes in lenticular stiffness even in the presence of no oxidative damage. The H_2O_2 group was the positive control, showing the direct effect of oxidative damage on lenticular biomechanical properties. The H_2O_2→PBS group was a positive control group to demonstrate that PBS cannot ameliorate or reverse oxidative damage. The H_2O_2→ALA group was the primary experimental group, showing that ALA could reduce or reverse oxidative damage induced changes to lens stiffness. I performed preliminary experiments with 12-, 9-, 6-, and 3-hour increments and found that I could detect elasticity changes even at 3 hour increments.

IV.2.3 Optical Properties Measurements

The pictures of the lenses in different media were taken by a standard dissection microscope (Stemi 508, Carl Zeiss Microscopy, LLC, Thornwood, NY, USA). For quantitative assessments of the changes in optical transparency, the OCT images were utilized to calculate the reciprocal of the OCT signal slope [109], referred to here as the attenuation, to quantify the opacity of the lenses. One hundred A-lines taken from the center of the lens were averaged for the calculation to eliminate artifacts in the calculations due to sensitivity roll-off and defocusing. The A-lines were averaged for each sample, and least-squares linear fit was performed to calculate the OCT signal slope. The selected region was 112 μm below the surface to avoid the influence of the specular reflection and

the linear fit was over 1.68 mm, which was where the intensity was indistinguishable from the background noise.

IV.2.4 Surface Wave Measurements

The extracted lenses were placed in the home-made lens holder. During OCE measurements, the lenses were half-submerged in 1X PBS, and an additional 1X PBS was topically dropped on the upper surface of the lenses every 20 seconds to make sure the lenses were hydrated. The focused air-pulse was targeted at the apex of the lens. The air-pulse induced a low amplitude localized displacement (≤10 μm) at the surface of the lens, which then propagated as an elastic wave. The SD-OCT system acquired successive M-mode images (n = 251) over a ~6.1 mm line [86], where the center of the scan was at the apex of the lens. The scan time for one position was approximately 10 ms, and the entire M-B scan time was approximately 30 s. The lenses were placed on a hollow tube with diameter of 7.3 mm. The raw temporal phase profiles were unwrapped, converted to displacement, and corrected for surface motion and refractive index mismatch artefacts [112]. The displacement profiles along the propagation path (i.e., along the curvature of the sample) were then processed by a cross-correlation algorithm to obtain the elastic wave propagation delays [87]. In short, the displacement profile at the excitation was used as a reference profile, and the displacement profiles from successively more distant positions were then cross-correlated with the reference profile. The peak of the subsequent cross-correlation was selected as the temporal delay for the elastic wave propagation to that OCE measurement position. A linear fit was then performed on the elastic wave propagation delays and their corresponding distances (incorporating the curvature of the sample). The speed of the elastic wave was converted to Young's modulus, *E*, by the surface wave

equation for incompressible material Eq. 2.1. Before measurements, all porcine lenses were physically measured with callipers, and there were no detectable changes in sample geometry during storage.

IV.3 Results

IV.3.1 Lens Transparency Analysis

Figure 4.2 shows images taken by a standard dissection microscope (Stemi 508, Carl Zeiss Microscopy, LLC, Thornwood, NY, USA) of the lenses in different media. As shown in Figure 4.2, the lenses incubated in PBS and the ALA solution did not show any apparent changes in the transparency, even after 9 hours. However, for the lenses incubated in the 500 mM hydrogen peroxide solution, the transparency was noticeably reduced. The most opaque lenses were the lenses incubated with H_2O_2 for 9 hours, as expected. The lenses that were placed in PBS after 3 hours incubation in H_2O_2 became more transparent at 6 hours and 9 hours. Moreover, lenses incubated with the ALA solution after 3 hours incubation in the H_2O_2 solution became clearer after 6 hours and 9 hours than the lenses that were incubated in only PBS after incubation in the hydrogen peroxide solution, suggesting that ALA may be more effective in reversing the oxidative effects of H_2O_2 than PBS.

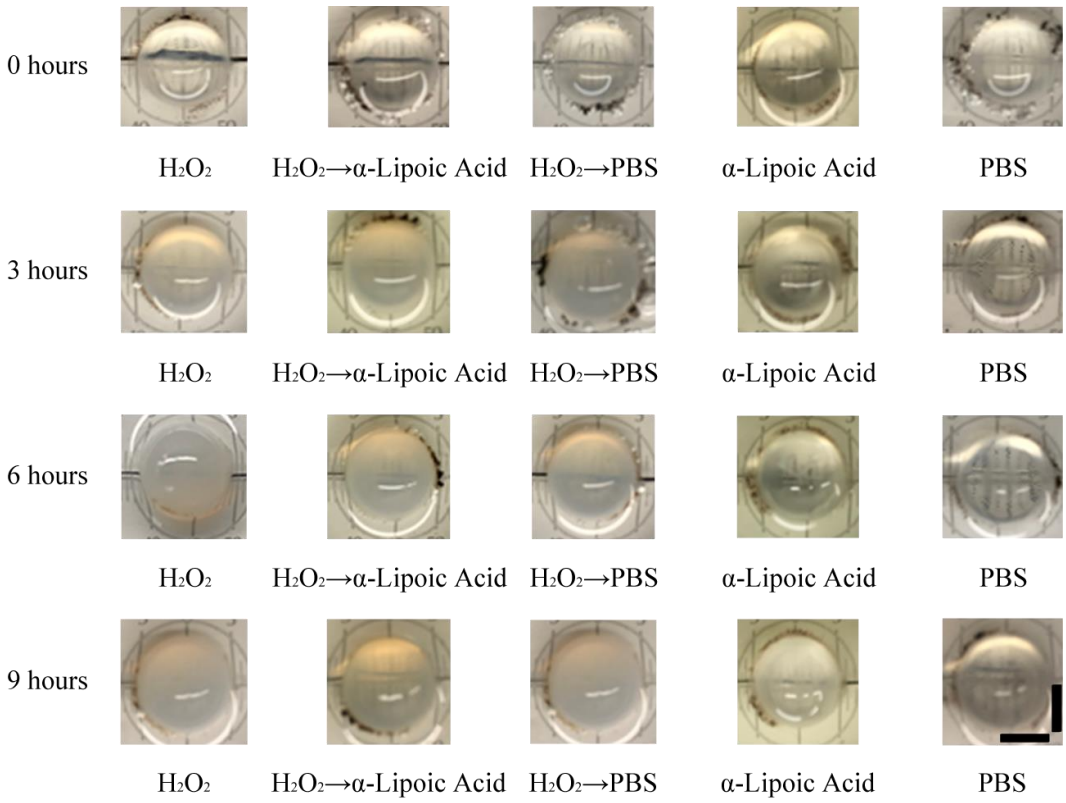

Figure 4.2. Photos of the lenses as a function of time and incubation media. The lenses at (top row) 0 hours, (second row) 3 hours, (third row) 6 hours, and (fourth row) 9 hours incubation time in the noted media. The scale bar is 5 mm.

Figure 4.3 plots the results of quantitative analysis of the changes in optical transparency for all of the samples. As the opacity of the lenses seen in Figure 4.2 increased, the scattering in the OCT image increased, resulting in greater attenuation. Statistical testing by a one-way ANOVA showed that the attenuation was not significant as a function of time for the two H_2O_2-free groups and H_2O_2→PBS group ($p > 0.05$), but was significant for the H_2O_2-only ($p = 0.005$) and H_2O_2→ALA groups ($p = 0.048$). These results indicate that the H_2O_2→ALA media change helped the lenses recover their transparency, while the H_2O_2→PBS group did not recover its transparency. This is clear from Figure 4.3, where there H_2O_2→ALA group decreases its attenuation much more quickly than the H_2O_2→PBS after the media change at 3 hours. At 9 hours after incubation, there was a significant

different in the attenuation of the H_2O_2-only (p = 0.004) and H_2O_2→PBS (p = 0.023) groups as compared to the PBS-only samples, but not in the H_2O_2→ALA (p = 0.34) and ALA-only (p = 0.65) groups as compared to the PBS-only samples.

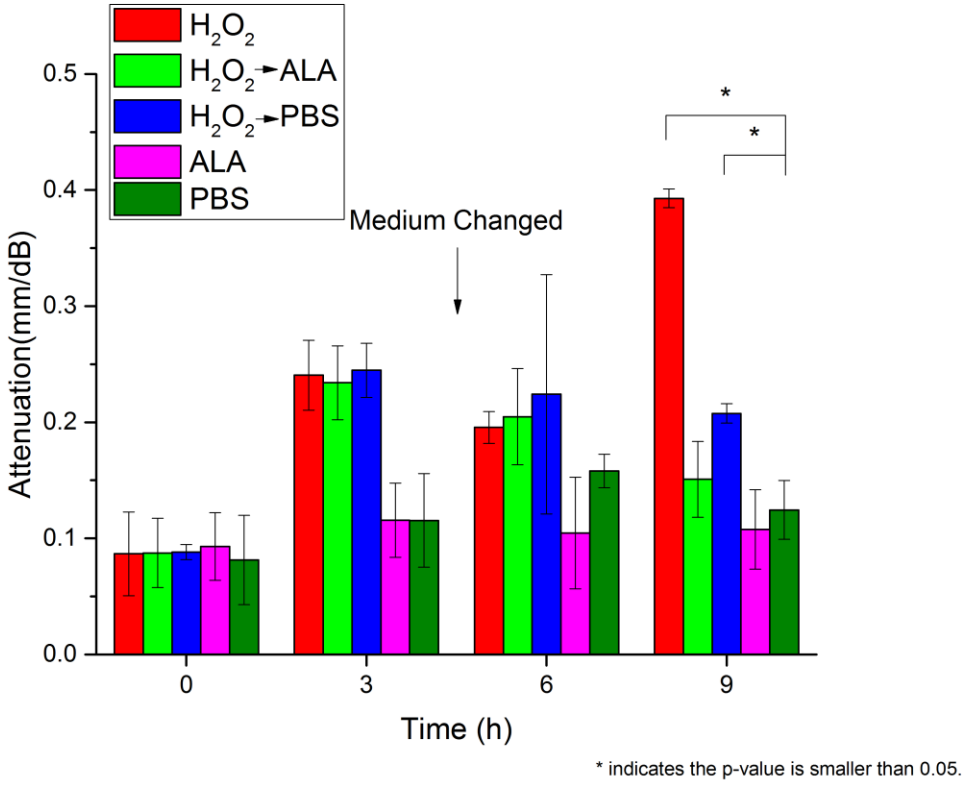

Figure 4.3. The attenuation calculated from the OCT images of the lenses incubated with five different media. The data is presented at the intersample mean ± standard deviation (N = 3 for each group). The asterisks indicate statistical significance.

IV.3.2 OCE Measurement of the Lenticular Biomechanical Properties

Figure 4.4 shows the space-time maps of two representative samples. Figure 4.4(a) was a sample from the H_2O_2→PBS group, and the elastic wave group velocity was 3.68 m/s. A space-time map of the elastic wave propagation in a sample from H_2O_2→ALA group is shown in Figure 4(b), where the group velocity of the elastic wave was 2.32 m/s.

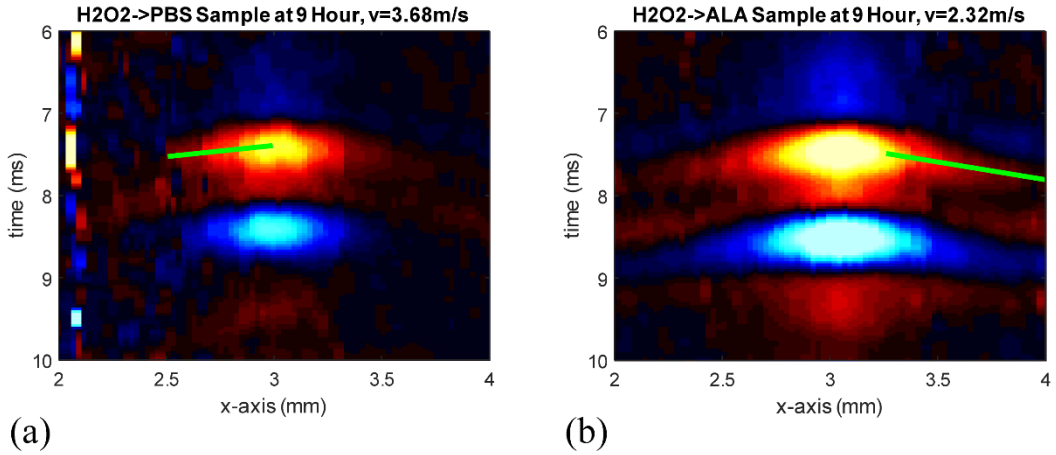

Figure 4.4. Space-time maps of one (**a**) H_2O_2→PBS and (**b**) H_2O_2→ALA lens at nine hours. The elastic wave propagation velocity was (**a**) 3.68 m/s and (**b**) 2.32 m/s.

Figures 4.5 and 4.6, as well as Table 4.1, show the OCE-measured group velocities and Young's moduli estimated using Equation 4.1 for different storage media and times of incubation. The elastic wave group velocity of three H_2O_2 groups started increasing compared to the two other groups after 6 hours of incubation. After 9 hours, the elastic wave propagated much more quickly in the H_2O_2-only group and H_2O_2→PBS groups, and the wave speed was also greater, albeit less so, in the H_2O_2→ALA group as compared to the H_2O_2-free groups. The elastic wave group velocity did not change much. Those two H_2O_2-free groups (PBS group and ALA group) did not change their group velocities much during the 9-hour incubation. Because the Young's moduli were calculated from group velocities. The major relationship among the Young's moduli of the five groups were similar.

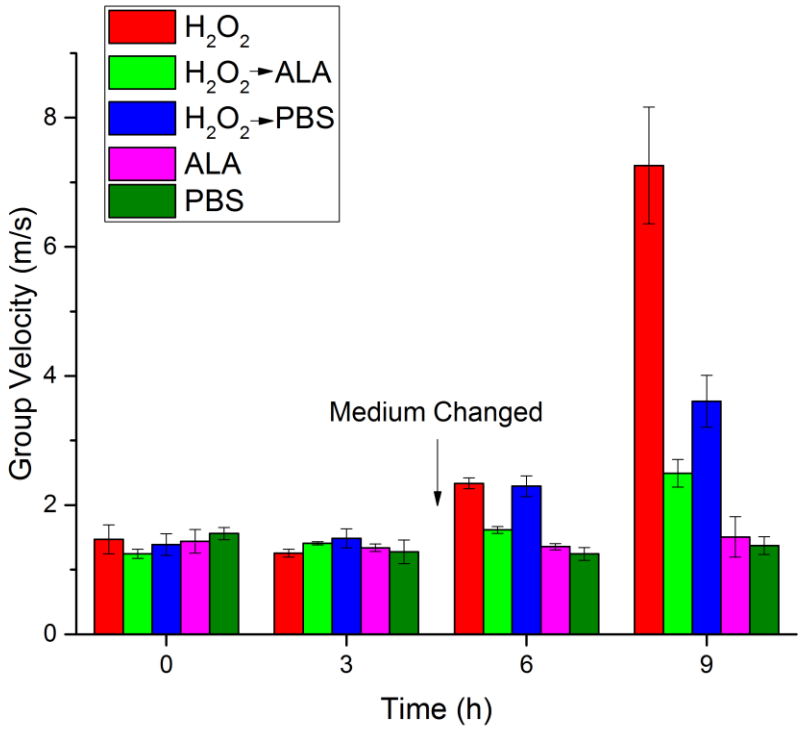

Figure 4.5. The surface wave group velocities measured in the lenses incubated with five different media. The data is presented at the inter-sample mean ± standard deviation (N = 3 for each group).

The Young's modulus of the lenses incubated only in H_2O_2 solution for 9 hours was significantly different from other groups ($p < 0.001$ by t-test). The Young's modulus of the lenses incubated in H_2O_2 and then ALA solution increased significantly from 0 hours to 9 hours by one-way ANOVA test ($p < 0.001$). The lenses incubated in H_2O_2 and then PBS media also showed an increase in Young's modulus at 0 hours and at 9 hours by one-way ANOVA test ($p < 0.001$). Meanwhile, Young's moduli of the lenses that were incubated with PBS did not change significantly by one-way ANOVA test ($p = 0.10$) for 9 hours. In addition, there was a statistically significant difference in Young's modulus between the lenses stored in PBS and ALA solutions after incubation in H_2O_2 solution at the final 9-

hour measurement by Student's t-test ($p = 0.04$). Data for the wave velocities and Young's moduli are summarized in Table 4.1.

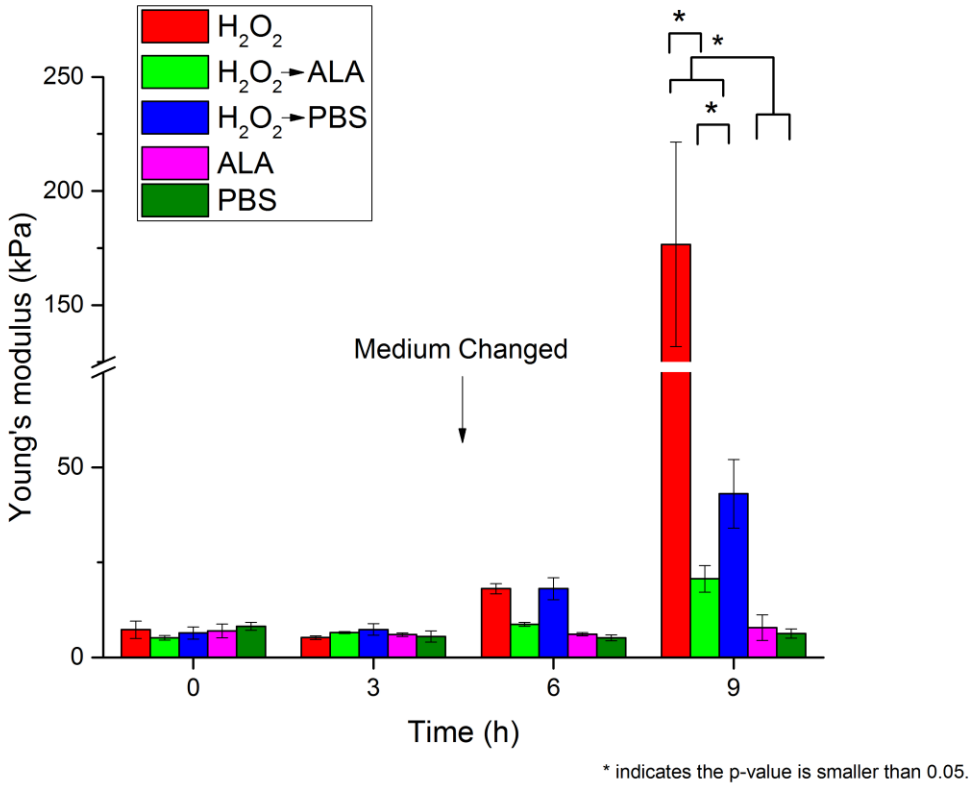

Figure 4.6. The OCE-estimated Young's moduli for the lenses incubated with five different media. The data are presented at the intersample mean ± standard deviation (N = 3 for each group). The asterisks indicate statistical significance.

Table 4.1. Surface wave group velocities and Young's moduli of the lenses incubated in different storage media. The error is the intersample standard deviation.

	0 h		**3 h**		**6 h**		**9 h**	
	c_g **(m/s)**	E **(kPa)**	c_g **(m/s)**	E **(kPa)**	c_g **(m/s)**	E **(kPa)**	c_g **(m/s)**	E **(kPa)**
H_2O_2	1.47 ± 0.22	7.28± 2.29	1.26 ± 0.06	5.21± 0.51	2.34 ± 0.08	18.09± 1.33	7.26 ± 0.90	176.62 ± 44.86
H_2O_2 → ALA	1.25 ± 0.07	5.15± 0.60	1.41 ± 0.03	6.55± 0.25	1.62 ± 0.05	8.69± 0.55	2.49 ± 0.21	20.67 ± 3.51
H_2O_2 → PBS	1.39 ± 0.17	6.44± 1.61	1.49 ± 0.15	7.35± 1.51	2.29 ± 0.16	18.08± 2.87	3.61 ± 0.40	43.03 ± 8.99
ALA	1.44 ± 0.18	6.95± 1.80	1.34 ± 0.06	5.98± 0.51	1.36 ± 0.05	6.12± 0.44	1.51 ± 0.31	7.82 ± 3.38
PBS	1.56 ± 0.09	8.18± 1.06	1.28 ± 0.18	5.54± 1.47	1.25 ± 0.10	5.17± 0.78	1.37 ± 0.14	6.28± 1.21

IV.4 Discussion

The oxidative cataract drastically alters not only the transparency but also biomechanical properties of the lens. OCE is well suited to investigate the changes in the crystalline lens associated with cataract onset, progression, and potential treatment. In this chapter, the surface wave velocity and Young's modulus of the lens during oxidative cataractogenesis were measured, and a significant increase in the stiffness of the cataract lenses was observed. The most dramatic changes occurred between 6 and 9 hours of incubation, even if the lenses were stored in the H_2O_2 medium for the first 3 hours only. After more than 9 hours of incubation in hydrogen peroxide, the lenses started to

demonstrate some plastic behaviour. The lenses are losing their elasticity and become very stiff. Although the relationship between lens stiffness and age is currently well known [32, 81, 99, 100, 105], studies on the influence of cataract formation on lens stiffness are still limited [81, 147]. Based on my previous results in Chapter III and this study, both cold and oxidative cataracts cause the lens to become stiffer, and the changes in stiffness correlate with the changes in lens opacity [36].

As shown in Figures 4.2 and 4.3, my results are in agreement with the literature, where the protective effect of ALA has been demonstrated [139-144]. The present study shows that the protective effect of ALA includes weakening of the stiffening caused by oxidative cataract. The results show a statistically significant difference between Young's modulus of the lenses stored in PBS and ALA media after incubation in H_2O_2 solution for 3 hours (43.03 ± 8.99 kPa versus 20.67 ± 3.51 kPa), which is in agreement with the work [9], where the decrease in the stiffness of the eight-month-old lenses after ALA treatment was shown in a mouse model. However, no statistically significant difference between control groups stored only in PBS and ALA media was observed in my results. This could be because the porcine lenses used in my study were obtained from relatively young animals, which did not have significant age-related changes in the biomechanical properties. Evaluating the effects of ALA on the aging-related biomechanical properties of the lens is the next step of my work.

Figures 4.2 and 4.3 show how the optical changes of the lens started at the 3-hour point. However, Figures 4.5 and 4.6 demonstrate that the mechanical changes of the lens started at 6 hours after incubation in the media. Varma et al. applied a 2-hour interval and the reactive oxygen species starts to make sense after 2 hours [148]. Because GSH is abundant

in epithelium and the outer cortex, it needs some time to consume the inner reductant for ALA to show effects. Interestingly, after the treatment of ALA, the optical properties recovered, but the changes in lenticular stiffness persisted. Due to high concentration of H_2O_2, the changes in opacities were observed in a very short time (3 hours). However, Spector et al. show that it took 72 hours for 0.2 H_2O_2 mM alter the transparency of lenses [149], which was 2000 times less concentrated than the solution used in this work. A next step of my work is to assess the changes in attenuation and elasticity at various concentrations to more rigorously determine the link between oxidative induced damage effects on optical transparency and biomechanical properties of the lens.

While my measurements were made on extracted lenses, OCE could be successfully used for the measurement of lens elasticity *in situ* and *in vivo*. The values of the surface wave speed in this study are in agreement with the previous results of my lab obtained on both extracted lenses and *in situ* lenses, i.e., inside eye globe. To translate these values to Young's modulus values, I used a model of surface wave in a homogeneous elastic medium. Such a model, however, has significant limitations. The elasticity distribution inside the lens is inhomogeneous, and the stiffness gradient is especially pronounced in aged lenses [32, 104, 105]. Therefore, the measurements on the lens surface are less sensitive to the mechanical properties of the nucleus, the central part of the lens. Moreover, different models gave different value of Young's modulus in the previous research of some other groups. Hollman et al. has the results of 5~10 kPa [105]; Schachar et al. has the shear modulus of 6.2 Pa [37]; which means the Young's modulus is about 20 Pa; and my previous result shows the Young's Modulus is about 10 kPa [36]. However, since the trends are also important, I need to understand the absolute value based on my model to check the

availability of my model. To overcome such limitations and quantify elasticity distribution in the lens, I have demonstrated the combination of dynamic OCE with Brillouin microscopy [51]. Another limitation in the model was that the effect of viscosity was not considered, but viscosity could play a significant role in the process of wave propagation. The measurement of the elastic wave dispersion in the lens, not only group velocity, along with the development of an appropriate wave propagation model that incorporates the geometry of the lens and specific boundary conditions, is the focus in Chapter V.

IV.5 Conclusion

In this chapter, I first applied OCE to observe the elasticity of the lens during the oxidation process and mimic the oxidative cataract generation. Oxidative cataract was induced in *ex vivo* porcine lenses, and the lenticular stiffness was assessed using elastic wave-based OCE. The cataract lenses demonstrated a significant increase in stiffness and opaqueness. The results show that there is a relationship between the stiffness and transparency of the lenses, and α-lipoic acid may potentially preserve both stiffness and transparency of the lenses. Future work includes evaluating the effectiveness of α-lipoic acid *in vivo* using OCE.

CHAPTER V - Age-Related Changes in the Viscoelasticity of Rabbit Lens Characterized by Surface Wave Dispersion Analysis

In this chapter, I took lenticular viscosity into consideration and started to do *in situ* investigation. The viscoelastic properties of the young and mature rabbit lenses *in situ* were evaluated using wave-based optical coherence elastography (OCE). Surface waves in the crystalline lens were generated using acoustic radiation force (ARF) focused inside the eyeball. Surface-wave dispersion was measured with a phase-stabilized optical coherence tomography (OCT) system. Young's modulus and shear viscosity coefficient were quantified based on a Scholte wave model and a Rayleigh wave model. The results showed that both elasticity and viscosity were significantly different between the young and mature lenses. The Young's modulus of the lenses increased with age from 7.74±1.56 kPa (young) to 15.15±4.52 kPa (mature), and the shear viscosity coefficient increased from 0.55±0.04 Pa·s (young) and 0.86±0.13 Pa·s (mature). The results showed that the combination of ARF excitation, OCE imaging, and dispersion analysis was enabled non-destructive quantification of lenticular viscoelasticity in situ and shows promise for *in vivo* applications.

V.1 Introduction

During aging, the lenticular biomechanical properties play critical roles in the development of presbyopia, which results in the age-related loss of accommodation [11, 33, 150]. Previous studies have shown that aging leads to an increase in lens stiffness in many species, including humans [32, 48, 52, 99, 101, 105, 151-153]. This increase in stiffness means that the lens is less responsive to mechanical stretching forces during accommodation, which decreases the ability of the lens to change its shape and

accommodate [150, 154]. Despite the significant role of lenticular biomechanical properties in vision, there is a lack of currently available technologies that can safely and noninvasively measure lens biomechanical properties inside the globe. While the changes in lens elasticity have been investigated in detail [32, 48, 52, 99, 101, 105, 151], only a few studies have measured changes in the lens viscous properties with age [66, 104, 151]. Complete information about lens biomechanical properties, e.g., viscoelasticity, would enable a better understanding of accommodation and development of new approaches to restore accommodation [11, 155].

In the previous chapters, I used wave-based OCE to show the correlation between lens opacity and elasticity during cold cataract formation and oxidative cataract formation in an *ex vivo* porcine model [36, 156]. However, these wave-based measurements relied on the wave group velocity, which was heavily influenced by the frequency of the wave and can only provide estimates of elasticity.

On the other hand, spectral analysis of surface wave propagation can enable robust assessments of tissue viscoelasticity [157, 158], which could enhance biomechanical measurements of the lens. In this chapter, the viscoelasticity of rabbit crystalline lenses *in situ* were assessed by inducing mechanical waves with focused acoustic radiation force, which were then detected by a phase-stabilized OCE system. Dispersion analysis was combined with a Scholte wave propagation model and a Rayleigh wave model to quantify the viscoelasticity of the crystalline lenses.

V.2 Materials and Methods

V.2.1 Experimental Setup

To measure the rabbit lenticular biomechanical properties, I utilized a phase-stabilized swept-source ARF-OCE system, which combines OCT with a co-focused single-element ultrasound transducer. Figure 5.1 shows the schematic of the experimental setup. The OCE system was based on a swept source laser (SL131090, Thorlabs Inc., Newton, NJ) with a central wavelength of ~1300 nm, a bandwidth of ~100 nm, and sweep rate of 100 kHz. The axial resolution of the OCT system was approximately 8 μm. The full width at half maximum (FWHM) of the transverse Gaussian profile of the OCT beam at the imaging focal plane was approximately 14 μm. The displacement stability of the system was measured as 1.9 nm. The raw interference signal was resampled into the linear k domain followed by a fast Fourier transform. The phase data was extracted from the angle of the complex OCT data after Fourier transform. The phase data was then converted to real distance with a refractive index of the lens as 1.38 [159]. The signal received will be directly transformed by inverse Fourier transform on the interference fringes with linear k-space [160, 161]. The ARF transducer (ISO 304HP; CTS Valpey Corporation, Hopkinton, MA) had a diameter of approximately 15 mm and a focal length of about 19 mm operating at 3.5 MHz central frequency. A 3.5 MHz sinusoidal wave was generated by a function generator (DG4062; Rigol Technologies, Beijing, China) and was gated to produce five single-tone bursts from 500 Hz to 2500 Hz with a 100 Hz increment. The signal for the transducer was amplified using a power amplifier (350L; Electronics & Innovation Ltd., Rochester, NY, USA). The ARF remotely perturbed the anterior apical surface of the crystalline lens through the cornea and the aqueous humor of the eyeball. A 3D printed

cone was filled with ultrasound gel to couple the ARF from the transducer to the eye. Since the intraocular pressure (IOP) can have a noticeable effect on the lens stiffness, it was controlled at 10 mmHg with a closed-loop control system [162].

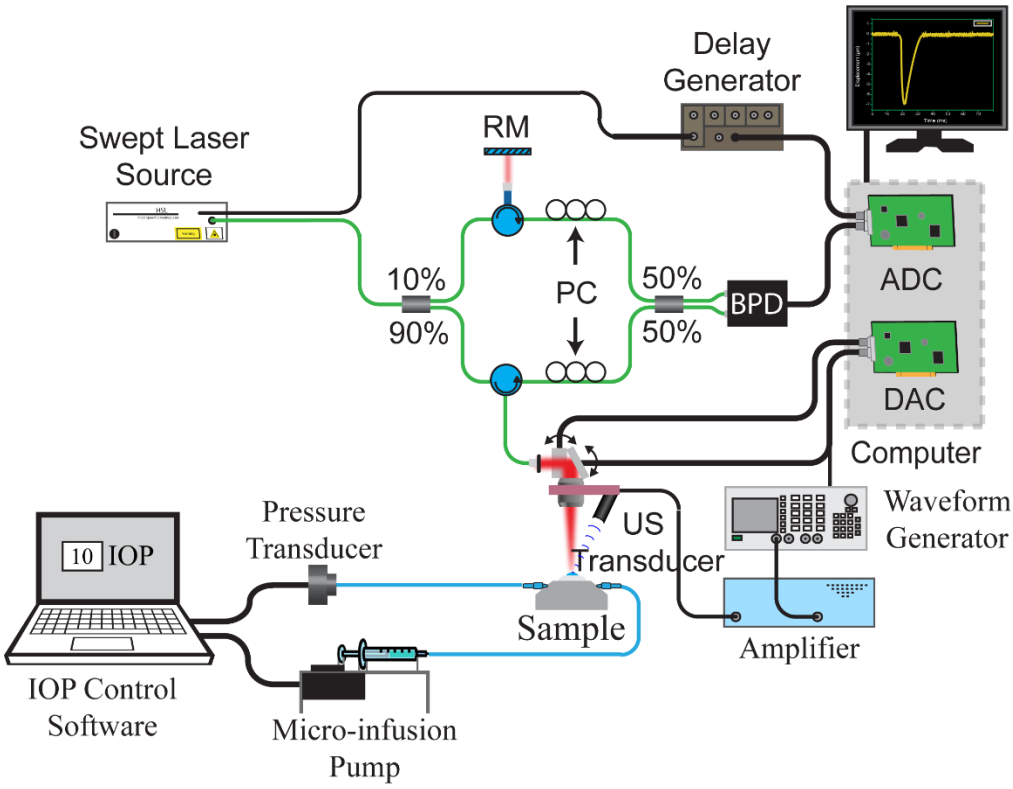

Figure 5.1. Schematic of the *in situ* US-OCE system

After the *in situ* measurements, the lenses were taken out and the measurements were done by another OCE system. The OCE system was based on a home-built spectral domain OCT (SDOCT), with an air-coupled ultrasound transducer [85, 163]. A schematic of the system is shown in Fig. 5.2. The SDOCT system utilized a superluminescent diode (SLD) with a central wavelength of ~840 nm, a bandwidth of ~49 nm. The displacement stability of the system was measured as 12 nm.

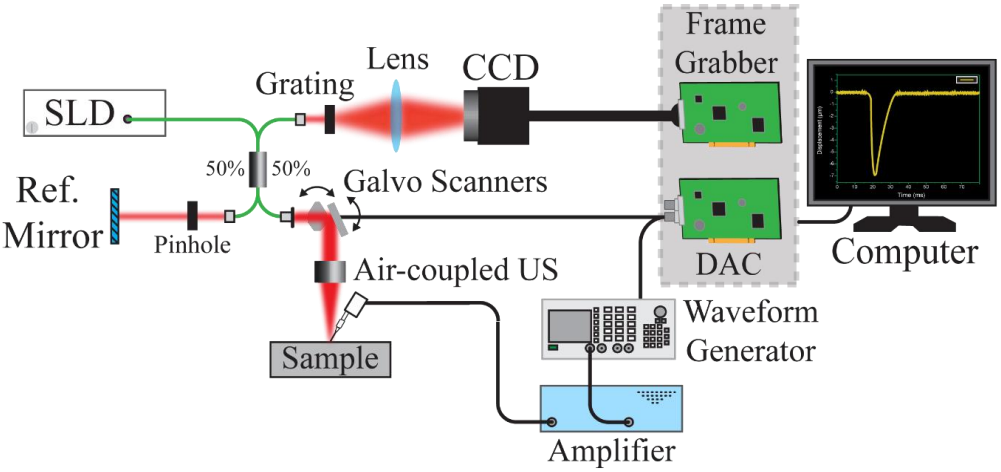

Figure 5.2. Schematic of the air-coupled US-OCE system

The transducer induced a low amplitude localized displacement (<10 μm) at the apical surface of the lens inside the eyeball (Fig. 5.3), which then propagated as an elastic wave. The OCE system acquired successive M-mode images (n=250) over a ~8.1 mm line, where the center of the scan was at the apex of the lens [86]. The scan time for one position was approximately 48 ms, and the entire M-B-mode scan time was about 12 s. The temporal phase profiles were unwrapped, converted to displacement, and corrected for surface compensation and refractive index mismatching artifacts [112]. The displacement profiles along the whole propagation path on the surface of the lens were then processed by a cross-correlation algorithm to obtain the elastic wave propagation delays [87] at each frequencies. The slope of a least-squares regression linear fit of the propagation delay to the propagation distance was the wave propagation speed. The fitting was performed from ~0.5 mm away from the excitation to remove the influence of near-field effects.

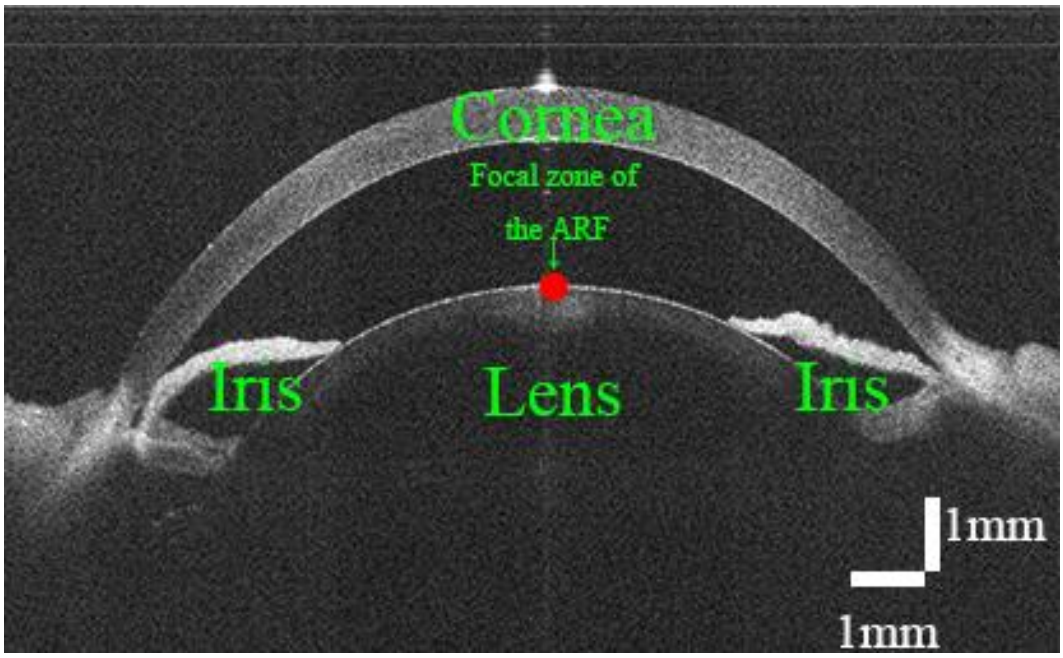

Figure 5.3. An OCT image of the lens *in situ*. The scale bar is 1 mm.

V.2.2 Sample Preparation

Whole rabbit eyes (Pel-Freez Biologicals, LLC, Rogers, AR) were shipped overnight on ice. The eyes were separated into two groups: young (from 2 to 3-months old, N=5) and mature (over 6-months old, N=10). All experiments were performed immediately after receiving the eyes. The eye globes were kept in a 1X PBS solution at room temperature to keep the globe hydrated. The samples were placed in a 3D-printed eye holder during the experiments to eliminate bulk motion and for IOP control as mentioned earlier. After the experiments, all lenses were enucleated to measure the size and mass. After the *in situ* measurements, the lenses were enucleated from the eyeballs and redid the measurements with air-coupled transducer as the previous publication of our lab described [163]. The lenses were placed on the holder and kept hydrated with PBS.

V.2.3 Wave Propagation Model

To evaluate age-related changes in the viscoelastic properties of the rabbit lenses quantitatively, I used a Kelvin-Voigt viscoelastic model of the tissue and Scholte wave model [164, 165], which matched the boundary conditions of the lens in the eye-globe (fluid on the anterior surface). I assumed that the lens thickness was significantly greater than mechanical wave wavelength in our frequency range (500-2500 Hz). The phase velocity of surface wave with a Kelvin-Voigt viscoelastic model of the tissue can be represented as

$$c_s(\omega) = \alpha \sqrt{\frac{2(\mu_1^2+\omega_s^2\mu_2^2)}{\rho(\mu_1+\sqrt{\mu_1^2+\omega_s^2\mu_2^2}}}, \tag{5.1}$$

where c_s is the measured phase velocity, ω is the angular frequency, $\rho = 1{,}183\ kg/m^3$ is the lens density [89], μ_1 is the shear modulus and μ_2 is the shear viscosity, α is the factor based on the model we applied, including $\alpha = 0.84$ for Scholte wave model and $\alpha = 0.95$ for Rayleigh wave model. After the measurements, Matlab (Mathworks, Natick, MA) curve fitting tool was used to fit the OCE measurements to the analytical model of wave propagation and estimate Young's modulus, *E*, based on the assumption of incompressibility (Eq. 1.6) [166].

V.3 Results

Table 5.1 shows the age, diameter, height, and mass of the lenses.

Table 5.1. The size and mass of the rabbit lenses.

	Young (N=5)	**Mature (N=10)**
Age (months)	2 to 3	>6
Diameter (mm)	5.98±0.42	7.99±0.52
Height (mm)	9.29±0.45	11.12±0.42
Mass (g)	0.33±0.07	0.70±0.07

Figure 5.4 shows the dispersion of the elastic wave (i.e., phase velocities) for representative lenses from (a) young rabbit group and (b) mature groups and their respective fitting curves obtained using Eq. 5.1. The phase velocity of the young lens went from ~1.4 m/s at 500 Hz to ~ 2.9 m/s at 2500 Hz. The phase velocity of the mature lens went from ~1.8 m/s at 500 Hz to ~ 3.4 m/s at 2500 Hz. Based on the curve fitting, the Young's modulus of the young lens was estimated as 6.6 kPa (95% confidence bounds [5.1, 7.8] kPa) and the shear viscosity was 0.54 Pa·s (95% confidence bounds [0.53, 0.56] Pa·s). The R^2 value of the fitting was 0.99. The Young's modulus of the mature lens was 15.6 kPa (95% confidence bounds [13.2, 17.7] kPa) and the shear viscosity was 0.83 Pa·s (95% confidence bounds [0.80, 0.85] Pa·s). The R^2 value of the fitting was 0.97.

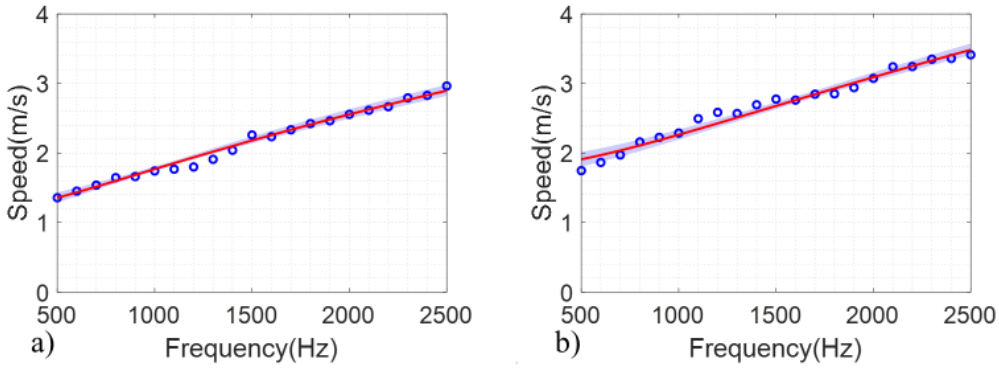

Figure 5.4. (blue circles) OCE-measured dispersion curves for the elastic wave propagation at the lens surface and (red line) fitting by the Scholte wave model for (a) one young lens and (b) one mature lens.

With the Young's modulus and the shear viscosity coefficient calculated by the curve fitting method, the average wave dispersion of each group of lenses was calculated. Figure 5.5 shows the average elastic wave dispersion curves for all lenses of each age group and their respective fitting to the mechanical model. It is obvious that the mature lenses had greater phase velocities in full frequency range than the young lens, indicating a greater stiffness.

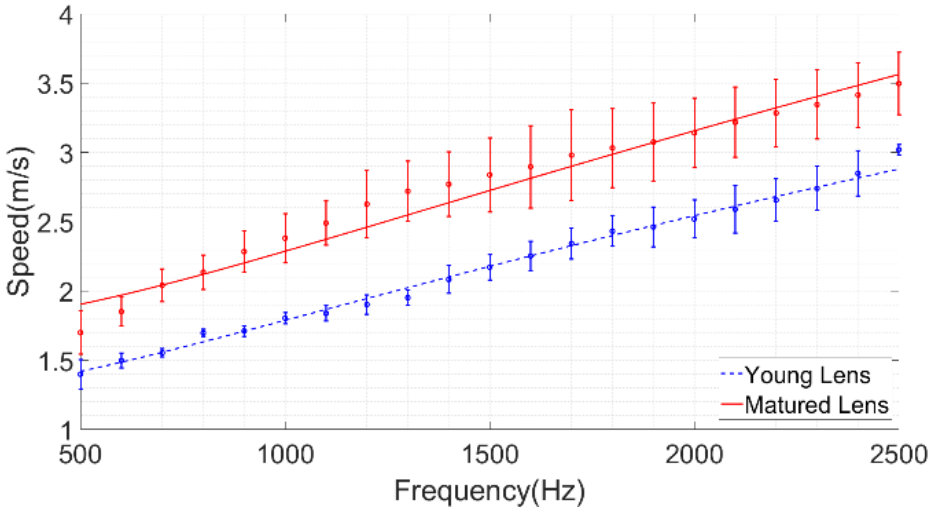

Figure 5.5. Average elastic wave dispersion curves of the young (N=5) and mature (N=10) lenses and the fit to the mechanical model using Eq. 5.1. The error bars show the intra-group standard deviation for each frequency.

The summary of the Young's modulus and the shear viscosity estimations is shown in Fig. 5.6. The results clearly show that the matured lenses are stiffer and more viscous than the young lenses, confirming our previous results with bovine lenses and rabbit lenses [66, 104]. Student's t-test was used to check the statistical significance of the difference between the two age groups. The average Young's modulus of the young lenses (7.74±1.56 kPa) was significantly lower than average Young's modulus of the mature lenses (15.15±4.52 kPa) ($P<0.001$). The shear viscosity coefficient of the young lenses (0.55±0.04 Pa·s) was also significantly lower than that of the matured lenses (0.86±0.13 Pa·s) ($P=0.013$). The trend is in agreement with our previous results in rabbit lenses based on the localized damping [66].

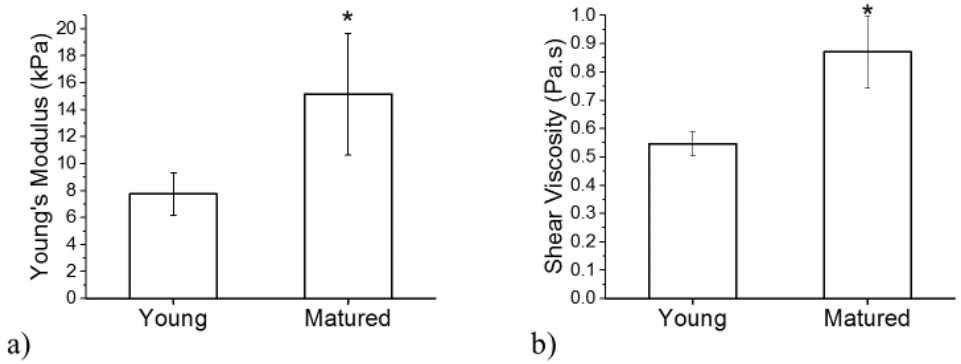

Figure 5.6. (a) Young's modulus and (b) shear viscosity coefficient of the young and mature lenses estimated based on the viscoelastic model. The asterisks indicate statistical significance ($P<0.05$) determined by Student's t-test.

Figure 5.7 shows the dispersion of the elastic wave (i.e., phase velocities) for representative young lenses from (a) inside the eyeball and (b) outside the eyeball and their respective fitting curves obtained using Eq. 5.1 by Scholte wave model and Rayleigh wave model. The phase velocity of the young lens inside went from ~1.4 m/s at 500 Hz to ~ 2.9 m/s at 2500 Hz. The phase velocity of the young lens outside went from ~1.4 m/s at 500 Hz to ~ 3.1 m/s at 2500 Hz. Based on the curve fitting, the Young's modulus of the young lens inside was estimated as 6.9 kPa (95% confidence bounds [4.5, 9.3] kPa) and the shear viscosity was 0.54 Pa·s (95% confidence bounds [0.52, 0.57] Pa·s). The R^2 value of the fitting was 0.96. The Young's modulus of the young lens outside was 6.3 kPa (95% confidence bounds [3.9, 8.7] kPa) and the shear viscosity was 0.47 Pa·s (95% confidence bounds [0.45, 0.50] Pa·s). The R^2 value of the fitting was 0.93.

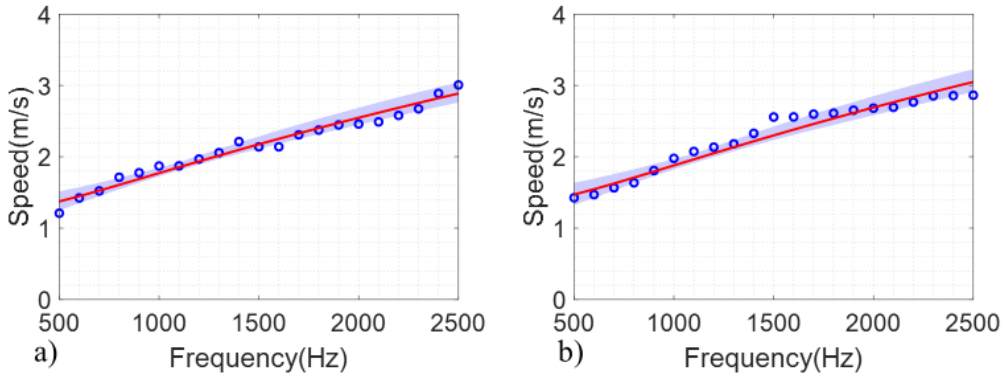

Figure 5.7. (blue circles) OCE-measured dispersion curves for the elastic wave propagation at the lens surface and (red line) fitting for one young lens (a) inside the eyeball and (b) outside the eyeball.

With the Young's modulus and the shear viscosity coefficient calculated by the curve fitting method, the average wave dispersion of young lenses inside or outside the eyeball was calculated. Figure 5.8 shows the average elastic wave dispersion curves for all young lenses inside or outside the eyeball and their respective fitting to the mechanical model. It is obvious that the lenses outside the eyeball had greater phase velocities in full frequency range than the lens inside the eyeball, indicating that Rayleigh waves propagate faster than Scholte waves (Eq. 5.1).

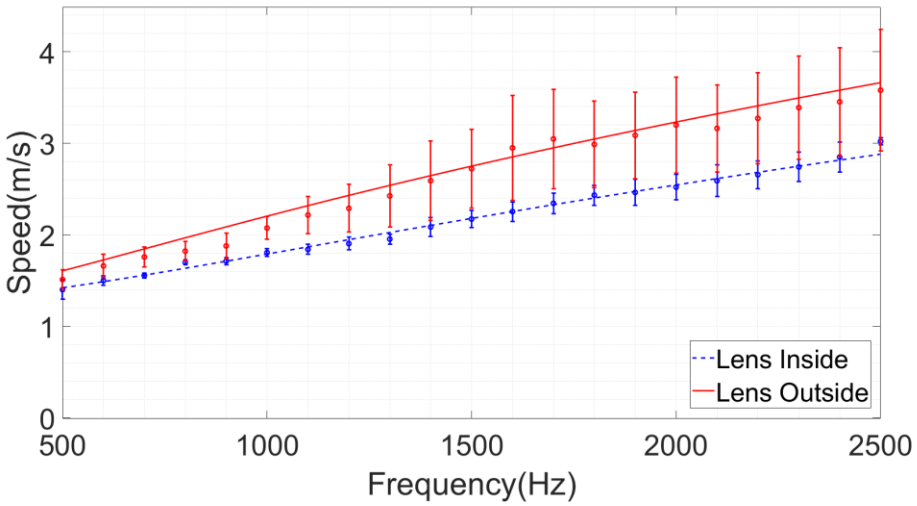

Figure 5.8. The estimated phase velocity dispersion curves of the young lens (N=5) inside and outside the eyeball. The error bars show the intra-group standard deviation for each frequency.

The summary of the Young's modulus and the shear viscosity estimations of the two models is shown in Fig. 5.9. The results clearly show that the lenticular properties calculated by two different models are not significantly different. Mann-Whitney test was used to check the statistical significance of the difference between the two models. The average Young's modulus of Scholte wave model (7.74±1.56 kPa) was not significantly different from average Young's modulus of Rayleigh wave model (5.98±1.06 kPa) (P=0.13). The shear viscosity calculated by Scholte wave model (0.55±0.04 Pa·s) was not significantly different from that calculated by Rayleigh wave model (0.65±0.11 Pa·s) (P=0.24). It shows that Scholte wave model and Rayleigh wave model can both be applied to evaluate young lenticular properties.

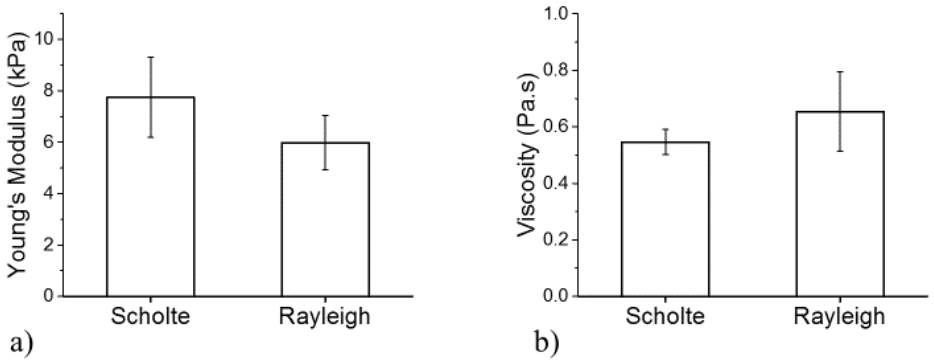

Figure 5.9. The (a) Young's modulus and (b) shear viscosity of the young lenses (N=5) estimated based on Scholte wave model and Rayleigh wave model. The asterisks indicate statistical significance ($p<0.05$) determined by t-test.

Figure 5.10 shows the dispersion of the elastic wave (i.e., phase velocities) for representative mature lenses from (a) inside the eyeball and (b) outside the eyeball and their respective fitting curves obtained using Eq. 5.1 by Scholte wave model and Rayleigh wave model. The phase velocity of the young lens inside went from ~1.8 m/s at 500 Hz to ~ 3.8 m/s at 2500 Hz. The phase velocity of the young lens outside went from ~2 m/s at 500 Hz to ~ 4.2 m/s at 2500 Hz. Based on the curve fitting, the Young's modulus of the young lens inside was estimated as 9.6 kPa (95% confidence bounds [6.6, 12.6] kPa) and the shear viscosity was 0.91 Pa·s (95% confidence bounds [0.88, 0.94] Pa·s). The R^2 value of the fitting was 0.98. The Young's modulus of the young lens outside was 9.0 kPa (95% confidence bounds [5.4, 12.6] kPa) and the shear viscosity was 0.88 Pa·s (95% confidence bounds [0.84, 0.92] Pa·s). The R^2 value of the fitting was 0.98.

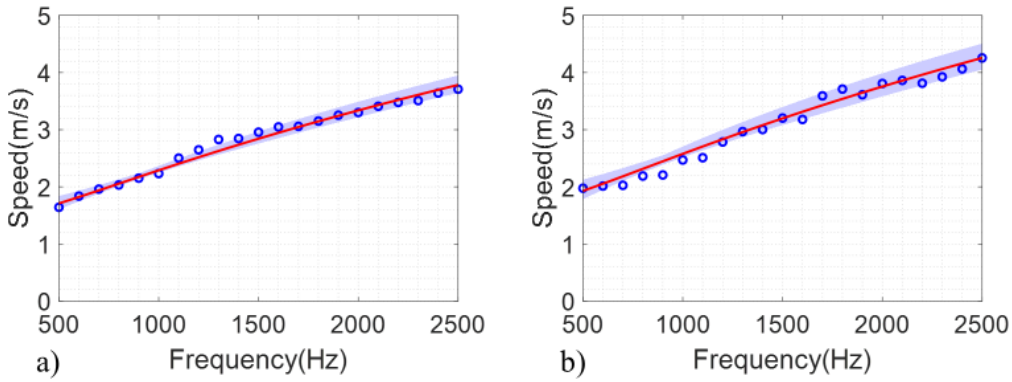

Figure 5.10. (blue circles) OCE-measured dispersion curves for the elastic wave propagation at the lens surface and (red line) fitting for one mature lens (a) inside the eyeball and (b) outside the eyeball.

With the Young's modulus and the shear viscosity coefficient calculated by the curve fitting method, the average wave dispersion of mature lenses inside or outside the eyeball was calculated. Figure 5.11 shows the average elastic wave dispersion curves for all mature lenses inside or outside the eyeball and their respective fitting to the mechanical model. The lenses outside the eyeball had slightly greater phase velocities in full frequency range than the lens inside the eyeball, indicating velocity data in Rayleigh wave model has higher number than velocity data in Scholte wave model.

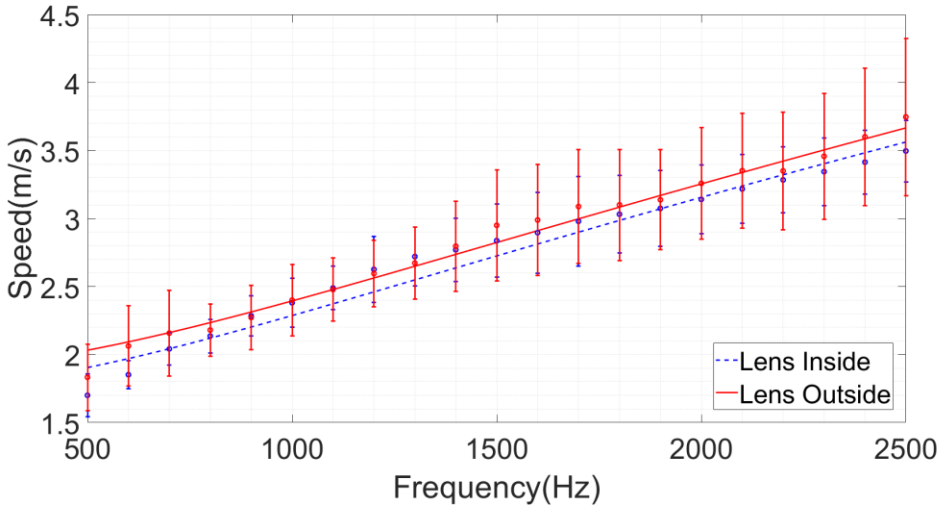

Figure 5.11. The estimated phase velocity dispersion curves of the mature lens (N=10) inside and outside the eyeball. The error bars show the intra-group standard deviation for each frequency.

Another summary of the Young's modulus and the shear viscosity estimations of the two models on mature lens is shown in Fig. 5.12. The results clearly show that the lenticular properties calculated by two different models are not significantly different. Mann-Whitney test was used to check the statistical significance of the difference between the two models. The average Young's modulus of Scholte wave model (15.15±4.52 kPa) was not significantly different from average Young's modulus of Rayleigh wave model (13.86±5.12 kPa) (P=0.13). The shear viscosity coefficient calculated by Scholte wave model (0.86±0.13 Pa·s) was not significantly different from that calculated by Rayleigh wave model (0.72±0.17 Pa·s) (P=0.16). It shows that Scholte wave model and Rayleigh wave model can both be applied to evaluate mature lenticular properties.

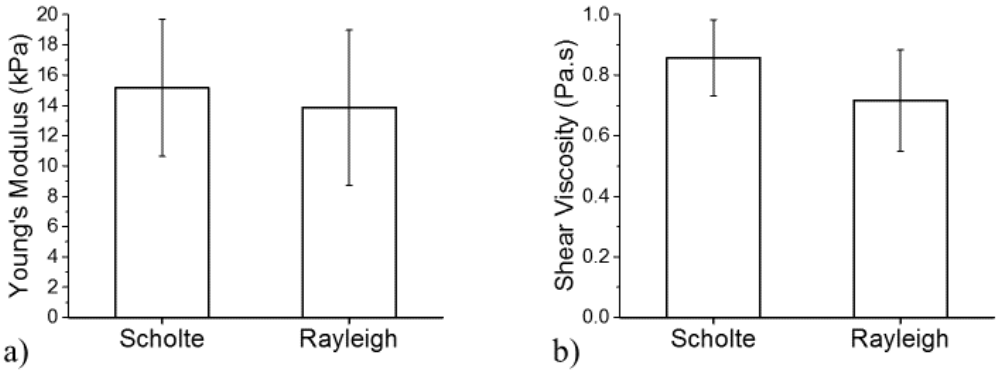

Figure 5.12. The (a) Young's modulus and (b) shear viscosity of the mature lenses (N=10) estimated based on Scholte wave model and Rayleigh wave model. The asterisks indicate statistical significance ($p<0.05$) determined by t-test.

V.4 Discussion

In this chapter, I utilized ARF to induce elastic waves at different frequencies in young and mature rabbit lenses *in situ* at a controlled IOP. The mechanical waves were detected by the OCE system, and the wave dispersion was utilized in an analytical model to quantify the viscoelasticity of the lenses. The results show that the mature lenses were stiffer and more viscous than the young lenses.

This tendency is in agreement with the results of the previous work of our lab, where the viscoelastic properties of the rabbit lenses were evaluated based on the measurement of the localized displacement temporal dynamics at the point of ARF excitation [66]. However, both the values of Young's modulus and shear viscosity coefficient obtained in this work are greater than in the previous results of our lab, where the Young modulus and shear viscosity coefficient were 2.5 kPa and 0.37 Pa·s, respectively, for the young lenses, and 7.4 kPa and 0.57 Pa·s for the mature lenses [66]. Still, in both studies the increase in stiffness with age is more pronounced than the increase in viscous coefficient. The difference in the estimated values could be explained by the difference in the measurement methods and the boundary conditions of the models. Previously, they used free boundary

conditions on the lens surface [66], while in this study more appropriate liquid-solid interaction was used.

One of the limitations of this surface wave-based technique is the limited ability to quantify the spatial distribution of the viscoelastic properties in the lens, particularly the stiffness gradient along the lens optical axis [32]. To overcome this limitation, the scholars have recently demonstrated a multimodal optical elastography technique based on OCE and Brillouin spectroscopy [167]. This method overcomes the depth limitations of OCE due to the limited optical scattering in the lens and the semi-quantitative nature of Brillouin spectroscopy.

My measurements were performed using the combined ARF-OCE system and air-coupled US-OCE system, and there are several different methods that can be applied to measure lenticular viscoelasticity, such as ultrasound elastography, uniaxial mechanical testing, and rheometry. Li et al. applied ARF-OCE to measure the elasticity of rabbit lenses of different age groups *in vivo*. Their results show that the 8-week old rabbit lens had a Young's modulus of ~10 kPa [152]. Wang et al. applied mechanical testing to measure the elasticity of the rabbit lens *ex vivo* and ultrasound elastography to measure the elasticity of the rabbit lens *in vivo*. Mechanical testing results showed that the Young's modulus of 7-month old rabbit lenses was 16.16±1.85 kPa, and the ultrasound elastography measured the average Young's modulus of 2-month rabbit lens as ~6.75 kPa and that of 7-month rabbit lens was 15.87 kPa [153]. Zhang et al. also applied ultrasound elastography to measure the elasticity of the rabbit lens *in vivo*. Their results show that the average Young's modulus of the 2-month old rabbit lens was about 5.7 kPa, and that of the 5-month old rabbit lens was about 15.87 kPa [48]. All these studies demonstrate that the Young's modulus of the

rabbit lens increases during the aging process and had relatively similar results in age-matched samples where applicable.

Current studies of the lens viscosity are scarce and use different experimental and analytical approaches. Elrefaei et al. vibrated the rabbit lens in different ultrasound environments to measure lenticular viscosity. Their results shows that the viscosity coefficient of the rabbit lens did not exceed 0.3 Pa·s, but the authors did not note the age of the samples [168]. Schachar et al. used a shear rheometer on porcine lenses and estimated the viscosity coefficient as 0.16±0.1 Pa·s [37]. The same approach was used to determine the viscoelastic properties of fresh human lenses under 40 years of age [151], where the dynamic viscosity at 75 Hz was 0.33 Pa·s and 0.35 Pa·s for nucleus and cortex, respectively, but no significant age dependence was observed. Yoon et al. compared the viscoelastic properties of the young (6 month old) and mature (25~30 month old) bovine lenses based on the measurement of laser-induced microbubbles in the lens [104]. The shear viscosity coefficient of the mature lenses (1.32 ± 0.12 Pa·s) was greater than the young lenses (1.06 ± 0.12 Pa·s) [104]. Overall, comparison of literature data is limited by the small number of studies and a range of experimental methods, but the results do show relatively similar shear viscosity coefficients.

In addition to material properties, the geometry of the lens can affect mechanical property measurements. For example, Sorsby et al. found the radius of curvature of front surface of rabbit lens increased from 5.2±0.42 mm at 7-weeks age to 6.1±0.37 mm at 20-weeks age [169]. However, the arc length difference between the lenses of two ages was about 7.5%, which is much smaller than the difference between the phase velocities of the young and mature lenses of the same frequencies shown in Fig. 5.5. The axial length also

changes with age as Table 5.1 shows. However, the wave model utilized in this work assumes a semi-infinite medium. At the worst-case scenario, i.e., the lowest frequency and slowest wave speed, the mechanical wave wavelength is ~2.8 mm. Hence, the assumption of a semi-infinite medium is reasonably sound given that the mechanical wave wavelength is greater than the thickness. Therefore, the curvature of the lens during the growth may not be considered as a key factor affecting the phase velocities of the lens.

V.5 Conclusion

In this chapter, I first applied OCE to measure the dispersion of the surface waves in rabbit crystalline lenses *in situ*. The elastic and viscous moduli of the lenses were significantly greater in the mature lenses as compared to the young lenses. The results show that the combination of ARF and OCE can be effectively used to quantify the age-related changes in lens viscoelasticity noninvasively. My future work is focused on *in vivo* measurements and the development of more robust mechanical wave models.

CHAPTER VI - Conclusion

The dissertation demonstrates a series of applications of noninvasive detection methods to characterize lens tissues from optical coherence elastography. Specifically, the work can be summarized into the following four chapters:

1) Assessing the effects of storage medium on the biomechanical properties of porcine lens with optical coherence elastography;

2) Optical coherence elastography of cold cataract in porcine lens;

3) Elasticity changes in the crystalline lens during oxidative damage and the antioxidant effect of alpha-lipoic acid measured by optical coherence elastography;

4) Age-Related changes in the viscoelasticity of rabbit lens characterized by surface wave dispersion analysis.

This dissertation represents the frontier of the OCE from their applications. The contribution of this dissertation research lies in biomechanical optics and they are about low coherence light interference. Crystalline lens is an essential organ of human eyes. The work presented in this dissertation can act as a foundation for the further development and the future applications of the techniques. The techniques and methods can be both applied in biological research and clinical or pre-clinical fields.

To spread, my methods can not only be used on lens, but can also be used for some other tissues, like cornea, retina, and so on.

References

[1] A. Banh, V. Bantseeva, V. Choh, K. L. Moran, and J. G. Sivak, "The lens of the eye as a focusing device and its response to stress," Progress in Retinal and Eye Research, 25(2), 189-206 (2006).

[2] R. P. Hemenger, L. F. Garner, and C. S. Ooi, "Change with Age of the Refractive-Index Gradient of the Human Ocular Lens," Investigative Ophthalmology & Visual Science, 36(3), 703-707 (1995).

[3] R. A. Gordon, and P. B. Donzis, "Refractive Development of the Human-Eye," Archives of Ophthalmology, 103(6), 785-789 (1985).

[4] J. Fernandez, M. Rodriguez-Vallejo, J. Martinez, A. Tauste, and D. P. Pinero, "From Presbyopia to Cataracts: A Critical Review on Dysfunctional Lens Syndrome," Journal of Ophthalmology, 2018, (2018).

[5] R. J. W. Truscott, and X. J. Zhu, "Presbyopia and cataract: A question of heat and time," Progress in Retinal and Eye Research, 29(6), 487-499 (2010).

[6] R. F. Fisher, "The elastic constants of the human lens," The Journal of Physiology, 212(1), 147-80 (1971).

[7] R. F. Fisher, "The mechanics of accommodation in relation to presbyopia," Eye, 2 (Pt 6), 646-9 (1988).

[8] R. Manapuram, S. Baranov, V. Manne, N. Sudheendran, M. Mashiatulla, S. Aglyamov, S. Emelianov, and K. Larin, "Assessment of wave propagation on

surfaces of crystalline lens with phase sensitive optical coherence tomography," Laser Physics Letters, 8(2), 164 (2010).

[9] W. H. Garner, and M. H. Garner, "Protein Disulfide Levels and Lens Elasticity Modulation: Applications for Presbyopia," Investigative Ophthalmology & Visual Science, 57(6), 2851-63 (2016).

[10] B. R. Masters, [Noninvasive diagnostic techniques in ophthalmology] Springer, (1990).

[11] A. Glasser, "Restoration of accommodation: surgical options for correction of presbyopia," Clinical and Experimental Optometry, 91(3), 279-295 (2008).

[12] H. Lubatschowski, S. Schumacher, M. Fromm, A. Wegener, H. Hoffmann, U. Oberheide, and G. Gerten, "Femtosecond lentotomy: generating gliding planes inside the crystalline lens to regain accommodation ability," Journal of Biophotonics, 3(5-6), 265-268 (2010).

[13] T. Ripken, U. Oberheide, M. Fromm, S. Schumacher, G. Gerten, and H. Lubatschowski, "fs-Laser induced elasticity changes to improve presbyopic lens accommodation," Graefes Archive for Clinical and Experimental Ophthalmology, 246(6), 897-906 (2008).

[14] S. Schumacher, U. Oberheide, M. Fromm, T. Ripken, W. Ertmer, G. Gerten, A. Wegener, and H. Lubatschowski, "Femtosecond laser induced flexibility change of human donor lenses," Vision Research, 49(14), 1853-1859 (2009).

[15] V. V. Tuchin, [Tissue optics] Society of Photo-Optical Instrumentation Engineers (SPIE), (2015).

[16] T. Niendorf, T. Huelnhagen, L. Winter, and K. Paul, "Human Cardiac Magnetic Resonance at Ultrahigh Fields: Technical Innovations, Early Clinical Applications and Opportunities for Discoveries," Cardiovascular Magnetic Resonance, 142-160. e4 (2019).

[17] R. C. Chivers, "Tissue Characterization," Ultrasound in Medicine and Biology, 7(1), 1-20 (1981).

[18] T. Cheng, J. Deng, S. Xiong, S. Yu, B. Zhang, J. Wang, W. Gong, H. Zhao, M. Luan, M. Zhu, J. Zhu, H. Zou, X. Xu, X. He, and X. Xu, "Crystalline Lens Power and Associated Factors in Highly Myopic Children and Adolescents Aged 4 to 19 Years," American Journal of Ophthalmology, 223, 169-177 (2021).

[19] C. H. Chien, T. Huang, and R. A. Schachar, "Analysis of human crystalline lens accommodation," Journal of Biomechanics, 39(4), 672-80 (2006).

[20] I. V. Turchin, "Methods of biomedical optical imaging: from subcellular structures to tissues and organs," Physics-Uspekhi, 59(5), 487-501 (2016).

[21] S. Pal, [Mechanical properties of biological materials] Springer, (2014).

[22] N. Özkaya, and M. Nordin, [Mechanical properties of biological tissues] Springer, (1999).

[23] S. Wang, and K. V. Larin, "Optical coherence elastography for tissue characterization: a review," Journal of Biophotonics, 8(4), 279-302 (2015).

[24] B. P. Danysh, and M. K. Duncan, “The lens capsule,” Experimental Eye Research, 88(2), 151-164 (2009).

[25] T. L. Beyer, G. Vogler, D. Sharma, and F. E. Odonnell, “Protective Barrier Effect of the Posterior Lens Capsule in Exogenous Bacterial Endophthalmitis - an Experimental Primate Study,” Investigative Ophthalmology & Visual Science, 25(1), 108-112 (1984).

[26] F. M. Tholozan, C. Gribbon, Z. Li, M. W. Goldberg, A. R. Prescott, N. McKie, and R. A. Quinlan, “FGF-2 release from the lens capsule by MMP-2 maintains lens epithelial cell viability,” Molecular Biology of the Cell, 18(11), 4222-31 (2007).

[27] C. J. Lee, J. A. Vroom, H. A. Fishman, and S. F. Bent, “Determination of human lens capsule permeability and its feasibility as a replacement for Bruch's membrane,” Biomaterials, 27(8), 1670-1678 (2006).

[28] O. A. Candia, “Electrolyte and fluid transport across corneal, conjunctival and lens epithelia,” Experimental Eye Research, 78(3), 527-535 (2004).

[29] H. Bloemendal, and O. Hockwin, “Lens protein,” Critical Reviews in Biochemistry, 12(1), 1-38 (1982).

[30] H. Bloemendal, W. de Jong, R. Jaenicke, N. H. Lubsen, C. Slingsby, and A. Tardieu, “Ageing and vision: structure, stability and function of lens crystallins,” Progress in Biophysics & Molecular Biology, 86(3), 407-485 (2004).

[31] D. L. Garland, Y. DouglasTabor, J. JimenezAsensio, M. B. Datiles, and B. Magno, “The nucleus of the human lens: Demonstration of a highly characteristic protein

pattern by two-dimensional electrophoresis and introduction of a new method of lens dissection," Experimental Eye Research, 62(3), 285-291 (1996).

[32] H. A. Weeber, G. Eckert, W. Pechhold, and R. G. van der Heijde, "Stiffness gradient in the crystalline lens," Graefe's Archive for Clinical and Experimental Ophthalmology, 245(9), 1357-66 (2007).

[33] J. F. Koretz, C. A. Cook, and P. L. Kaufman, "Accommodation and presbyopia in the human eye - Changes in the anterior segment and crystalline lens with focus," Investigative Ophthalmology & Visual Science, 38(3), 569-578 (1997).

[34] K. R. Heys, S. L. Cram, and R. J. Truscott, "Massive increase in the stiffness of the human lens nucleus with age: the basis for presbyopia?," Mol Vis, 10, 956-63 (2004).

[35] K. J. Dilley, and A. Pirie, "Changes to the proteins of the human lens nucleus in cataract," Experimental Eye Research, 19(1), 59-72 (1974).

[36] H. Zhang, C. Wu, M. Singh, A. Nair, S. Aglyamov, and K. Larin, "Optical coherence elastography of cold cataract in porcine lens," Journal of Biomedical Optics, 24(3), 1-7 (2019).

[37] R. A. Schachar, R. W. Chan, and M. Fu, "Viscoelastic shear properties of the fresh porcine lens," British Journal of Ophthalmology, 91(3), 366-368 (2007).

[38] R. M. S. Sigrist, J. Liau, A. E. Kaffas, M. C. Chammas, and J. K. Willmann, "Ultrasound Elastography: Review of Techniques and Clinical Applications," Theranostics, 7(5), 1303-1329 (2017).

[39] J. L. Gennisson, T. Deffieux, M. Fink, and M. Tanter, "Ultrasound elastography: principles and techniques," Diagnostic and Interventional Imaging, 94(5), 487-95 (2013).

[40] X. C. Pan, J. Siewerdsen, P. J. La Riviere, and W. A. Kalender, "Anniversary Paper: Development of x-ray computed tomography: The role of Medical Physics and AAPM from the 1970s to present," Medical Physics, 35(8), 3728-3739 (2008).

[41] W. A. Kalender, "X-ray computed tomography," Physics in Medicine and Biology, 51(13), R29-R43 (2006).

[42] S. M. Snyder, and E. Schneider, "Estimation of Mechanical-Properties of Cortical Bone by Computed-Tomography," Journal of Orthopaedic Research, 9(3), 422-431 (1991).

[43] S. A. Morris, and T. C. Slesnick, "Magnetic resonance imaging," Visual Guide to Neonatal Cardiology, 104-108 (2018).

[44] M. T. Vlaardingerbroek, and J. A. Boer, [Magnetic resonance imaging: theory and practice] Springer Science & Business Media, (2013).

[45] S. W. Young, "Magnetic resonance imaging: basic principles," (1987).

[46] J. Ophir, I. Cespedes, H. Ponnekanti, Y. Yazdi, and X. Li, "Elastography - a Quantitative Method for Imaging the Elasticity of Biological Tissues," Ultrasonic Imaging, 13(2), 111-134 (1991).

[47] D. V. Litwiller, S. J. Lee, A. Kolipaka, Y. K. Mariappan, K. J. Glaser, J. S. Pulido, and R. L. Ehman, "MR elastography of the ex vivo bovine globe," Journal of Magnetic Resonance Imaging, 32(1), 44-51 (2010).

[48] X. Y. Zhang, Q. M. Wang, Z. Lyu, X. H. Gao, P. P. Zhang, H. M. Lin, Y. R. Guo, T. F. Wang, S. P. Chen, and X. Chen, "Noninvasive assessment of age-related stiffness of crystalline lenses in a rabbit model using ultrasound elastography," BioMedical Engineering OnLine, 17, (2018).

[49] D. Touboul, J. L. Gennisson, T. M. Nguyen, A. Robinet, C. J. Roberts, M. Tanter, and N. Grenier, "Supersonic Shear Wave Elastography for the In Vivo Evaluation of Transepithelial Corneal Collagen Cross-Linking," Investigative Ophthalmology & Visual Science, 55(3), 1976-1984 (2014).

[50] A. L. Sheppard, C. J. Evans, K. D. Singh, J. S. Wolffsohn, M. C. Dunne, and L. N. Davies, "Three-dimensional magnetic resonance imaging of the phakic crystalline lens during accommodation," Investigative Ophthalmology & Visual Science, 52(6), 3689-97 (2011).

[51] Y. S. Ambekar, M. Singh, J. Zhang, A. Nair, S. R. Aglyamov, G. Scarcelli, and K. V. Larin, "Multimodal quantitative optical elastography of the crystalline lens with optical coherence elastography and Brillouin microscopy," Biomedical Optics Express, 11(4), 2041-2051 (2020).

[52] G. Scarcelli, P. Kim, and S. H. Yun, "In Vivo Measurement of Age-Related Stiffening in the Crystalline Lens by Brillouin Optical Microscopy," Biophysical Journal, 101(6), 1539-1545 (2011).

[53] S. Reiß, K. Sperlich, M. Hovakimyan, P. Martius, R. F. Guthoff, H. Stolz, and O. Stachs, “Ex vivo measurement of postmortem tissue changes in the crystalline lens by Brillouin spectroscopy and confocal reflectance microscopy,” IEEE Transactions on Biomedical Engineering, 59(8), 2348 (2012).

[54] A. de Castro, A. Benito, S. Manzanera, J. Mompean, B. Canizares, D. Martinez, J. M. Marin, I. Grulkowski, and P. Artal, “Three-Dimensional Cataract Crystalline Lens Imaging With Swept-Source Optical Coherence Tomography,” Investigative Ophthalmology & Visual Science, 59(2), 897-903 (2018).

[55] W. Drexler, U. Morgner, R. K. Ghanta, F. X. Kartner, J. S. Schuman, and J. G. Fujimoto, “Ultrahigh-resolution ophthalmic optical coherence tomography,” Nature Medicine, 7(4), 502-507 (2001).

[56] J. G. Fujimoto, W. Drexler, J. S. Schuman, and C. K. Hitzenberger, “Optical Coherence Tomography (OCT) in ophthalmology: introduction,” Optics Express, 17(5), 3978-9 (2009).

[57] D. Huang, E. A. Swanson, C. P. Lin, J. S. Schuman, W. G. Stinson, W. Chang, M. R. Hee, T. Flotte, K. Gregory, C. A. Puliafito, and J. G. Fujimoto, “Optical Coherence Tomography,” Science, 254(5035), 1178-1181 (1991).

[58] B. J. Kaluzny, J. J. Kaluzny, A. Szkulmowska, I. Gorczynska, M. Szkulmowski, T. Bajraszewski, M. Wojtkowski, and P. Targowski, “Spectral optical coherence tomography - A novel technique for cornea imaging,” Cornea, 25(8), 960-965 (2006).

[59] R. F. Spaide, J. G. Fujimoto, N. K. Waheed, S. R. Sadda, and G. Staurenghi, "Optical coherence tomography angiography," Progress in Retinal and Eye Research, 64, 1-55 (2018).

[60] C. L. Shields, M. A. Materin, and J. A. Shields, "Review of optical coherence tomography for intraocular tumors," Current Opinion in Ophthalmology, 16(3), 141-54 (2005).

[61] E. Sattler, R. Kastle, and J. Welzel, "Optical coherence tomography in dermatology," Journal of Biomedical Optics, 18(6), (2013).

[62] B. F. Kennedy, X. Liang, S. G. Adie, D. K. Gerstmann, B. C. Quirk, S. A. Boppart, and D. D. Sampson, "In vivo three-dimensional optical coherence elastography," Optics Express, 19(7), 6623-34 (2011).

[63] Y. Li, J. Zhu, J. J. Chen, J. Yu, Z. Jin, Y. Miao, A. W. Browne, Q. Zhou, and Z. Chen, "Simultaneously imaging and quantifying in vivo mechanical properties of crystalline lens and cornea using optical coherence elastography with acoustic radiation force excitation," APL Photonics, 4(106104), 1-10 (2019).

[64] C. Wu, S. R. Aglyamov, Z. L. Han, M. Singh, C. H. Liu, and K. V. Larin, "Assessing the biomechanical properties of the porcine crystalline lens as a function of intraocular pressure with optical coherence elastography," Biomedical Optics Express, 9(12), 6455-66 (2018).

[65] C. Wu, S. R. Aglyamov, C.-H. Liu, Z. Han, M. Singh, and K. V. Larin, "Biomechanical properties of crystalline lens as a function of intraocular pressure assessed noninvasively by optical coherence elastography." 10045, 1004503-1.

[66] C. Wu, Z. Han, S. Wang, J. Li, M. Singh, C.-h. Liu, S. Aglyamov, S. Emelianov, F. Manns, and K. V. Larin, "Assessing Age-Related Changes in the Biomechanical Properties of Rabbit Lens Using a Coaligned Ultrasound and Optical Coherence Elastography SystemAge-Related Changes in Biomechanics of Lens," Investigative Ophthalmology & Visual Science, 56(2), 1292-1300 (2015).

[67] R. K. Manapuram, N. Sudheendran, V. R. Manne, S. A. Baranov, S. Aglyamov, S. Emelianov, and K. V. Larin, "3D Assessment of Mechanical Wave Propagation in the Crystalline Eye Lens using PhS-SSOCT," Ophthalmic Technologies XXI, 7885, (2011).

[68] T. H.-T. Ko, [High speed data acquisition system for optical coherence tomograpy] Massachusetts Institute of Technology, (2000).

[69] D. Huang, F. Li, Z. He, Z. Cheng, C. Shang, and P. K. A. Wai, "400 MHz ultrafast optical coherence tomography," Optics Letters, 45(24), 6675-6678 (2020).

[70] A. F. Fercher, W. Drexler, C. K. Hitzenberger, and T. Lasser, "Optical coherence tomography - principles and applications," Reports on Progress in Physics, 66(2), 239-303 (2003).

[71] A. M. Zysk, F. T. Nguyen, A. L. Oldenburg, D. L. Marks, and S. A. Boppart, "Optical coherence tomography: a review of clinical development from bench to bedside," Journal of Biomedical Optics, 12(5), (2007).

[72] R. Leitgeb, C. K. Hitzenberger, and A. F. Fercher, "Performance of fourier domain vs. time domain optical coherence tomography," Optics Express, 11(8), 889-894 (2003).

[73] Z. Yaqoob, J. Wu, and C. Yang, "Spectral domain optical coherence tomography: a better OCT imaging strategy," BioTechniques, 39(6 Suppl), S6-13 (2005).

[74] J. M. Schmitt, "OCT elastography: imaging microscopic deformation and strain of tissue," Optics Express, 3(6), 199-211 (1998).

[75] B. F. Kennedy, K. M. Kennedy, and D. D. Sampson, "A Review of Optical Coherence Elastography: Fundamentals, Techniques and Prospects," Ieee Journal of Selected Topics in Quantum Electronics, 20(2), (2014).

[76] X. Liang, V. Crecea, and S. A. Boppart, "Dynamic Optical Coherence Elastography: A Review," Journal of Innovative Optical Health Sciences, 3(4), 221-233 (2010).

[77] V. Crecea, A. Ahmad, and S. A. Boppart, "Magnetomotive optical coherence elastography for microrheology of biological tissues," Journal of Biomedical Optics, 18(12), (2013).

[78] J. M. Carcione, [Wave fields in real media: Wave propagation in anisotropic, anelastic, porous and electromagnetic media] Elsevier, (2007).

[79] S. R. Aglyamov, [Chapter 2: The governing theory of elasticity imaging] Elsevier, 2 (2020).

[80] P. N. T. Wells, and H. D. Liang, “Medical ultrasound: imaging of soft tissue strain and elasticity,” Journal of the Royal Society Interface, 8(64), 1521-1549 (2011).

[81] K. R. Heys, and R. J. W. Truscott, “The stiffness of human cataract lenses is a function of both age and the type of cataract,” Experimental Eye Research, 86(4), 701-703 (2008).

[82] S. Wang, S. Aglyamov, A. Karpiouk, J. Li, S. Emelianov, F. Manns, and K. V. Larin, “Assessing the mechanical properties of tissue-mimicking phantoms at different depths as an approach to measure biomechanical gradient of crystalline lens,” Biomedical Optics Express, 4(12), 2769-2780 (2013).

[83] R. Brinkmann, B. Radt, C. Flamm, J. Kampmeier, N. Koop, and R. Birngruber, “Influence of temperature and time on thermally induced forces in corneal collagen and the effect on laser thermokeratoplasty,” Journal of Cataract & Refractive Surgery, 26(5), 744-754 (2000).

[84] S. Aglyamov, W. Shang, A. Karpiouk, L. Jiasong, M. Twa, S. Emelianov, and K. V. Larin, "Assessment of the depth-dependence of the mechanical parameters of a layered medium using surface excitation and motion measurements on the surface." 1252-1255.

[85] H. Zhang, C. Wu, M. Singh, and K. V. Larin, "Quantifying changes in lens biomechanical properties due to cold cataract with optical coherence elastography." 10474, 104741Y.

[86] S. Wang, and K. V. Larin, “Shear wave imaging optical coherence tomography (SWI-OCT) for ocular tissue biomechanics,” Optics Letters, 39(1), 41-44 (2014).

[87] S. Wang, A. L. Lopez, Y. Morikawa, G. Tao, J. S. Li, I. V. Larina, J. F. Martin, and K. V. Larin, “Noncontact quantitative biomechanical characterization of cardiac muscle using shear wave imaging optical coherence tomography,” Biomedical Optics Express, 5(7), 1980-1992 (2014).

[88] R. M. Christensen, [Theory of viscoelasticity. An Introduction.] Academic Press, New York and London(1971).

[89] A. S. Vilupuru, and A. Glasser, “Optical and biometric relationships of the isolated pig crystalline lens,” Ophthalmic and Physiological Optics, 21(4), 296-311 (2001).

[90] D. Pascolini, and S. P. Mariotti, “Global estimates of visual impairment: 2010,” British Journal of Ophthalmology, 96(5), 614-8 (2012).

[91] B. Singh, D. Kumar, and R. Singh, “Phytotherapeutics for management and prevention of cataract generation,” Phytopharmacology, 3(1), 93-110 (2012).

[92] R. J. Siezen, M. R. Fisch, C. Slingsby, and G. B. Benedek, “Opacification of gamma-crystallin solutions from calf lens in relation to cold cataract formation,” Proceedings of the National Academy of Sciences of the United States of America, 82(6), 1701-5 (1985).

[93] S. Zigman, and S. Lerman, “Properties of a cold-precipitable protein fraction in the Lens,” Experimental Eye Research, 4, 24-30 (1965).

[94] S. Lerman, and S. Zigman, “Metabolic studies on the cold precipitable protein of the lens,” Acta Ophthalmologica, 45(2), 193-199 (1967).

[95] T. Tanaka, C. Ishimoto, and L. T. Chylack, Jr., “Phase separation of a protein-water mixture in cold cataract in the young rat lens,” Science, 197(4307), 1010-2 (1977).

[96] J. G. Sivak, D. D. Stuart, and J. A. Weerheim, “Optical performance of the bovine lens before and after cold cataract,” Applied Optics, 31(19), 3616-3620 (1992).

[97] M. A. Loewenstein, and F. A. Bettelheim, “Cold cataract formation in fish lenses,” Experimental Eye Research, 28(6), 651-663 (1979).

[98] A. Banh, and J. G. Sivak, “Laser scanning analysis of cold cataract in young and old bovine lenses,” Molecular Vision, 10, 144-147 (2004).

[99] H. A. Weeber, G. Eckert, F. Soergel, C. H. Meyer, W. Pechhold, and R. G. van der Heijde, “Dynamic mechanical properties of human lenses,” Experimental Eye Research, 80(3), 425-34 (2005).

[100] S. Krag, and T. T. Andreassen, “Biomechanical measurements of the porcine lens capsule,” Experimental Eye Research, 62(3), 253-260 (1996).

[101] T. N. Erpelding, K. W. Hollman, and M. O'Donnell, “Mapping age-related elasticity changes in porcine lenses using bubble-based acoustic radiation force,” Experimental Eye Research, 84(2), 332-341 (2007).

[102] H. A. Weeber, and R. G. L. van der Heijde, “On the relationship between lens stiffness and accommodative amplitude,” Experimental Eye Research, 85(5), 602-607 (2007).

[103] H. J. Burd, G. S. Wilde, and S. J. Judge, “An improved spinning lens test to determine the stiffness of the human lens,” Experimental Eye Research, 92(1), 28-39 (2011).

[104] S. Yoon, S. Aglyamov, A. Karpiouk, and S. Emelianov, “The mechanical properties of ex vivo bovine and porcine crystalline lenses: age-related changes and location-dependent variations,” Ultrasound in Medicine and Biology, 39(6), 1120-7 (2013).

[105] K. W. Hollman, M. O'donnell, and T. N. Erpelding, “Mapping elasticity in human lenses using bubble-based acoustic radiation force,” Experimental Eye Research, 85(6), 890-893 (2007).

[106] S. Yoon, S. Aglyamov, A. Karpiouk, and S. Emelianov, “A high pulse repetition frequency ultrasound system for the ex vivo measurement of mechanical properties of crystalline lenses with laser-induced microbubbles interrogated by acoustic radiation force,” Physics in Medicine and Biology, 57(15), 4871-4884 (2012).

[107] S. Park, H. Yoon, K. V. Larin, S. Y. Emelianov, and S. R. Aglyamov, “The impact of intraocular pressure on elastic wave velocity estimates in the crystalline lens,” Physics in Medicine & Biology, 62(3), N45 (2017).

[108] E. F. Carbajal, S. A. Baranov, V. G. R. Manne, E. D. Young, A. J. Lazar, D. C. Lev, R. E. Pollock, and K. V. Larin, “Revealing retroperitoneal liposarcoma

morphology using optical coherence tomography," Journal of Biomedical Optics, 16(2), (2011).

[109] S. Wang, K. V. Larin, J. S. Li, S. Vantipalli, R. K. Manapuram, S. Aglyamov, S. Emelianov, and M. D. Twa, "A focused air-pulse system for optical-coherence-tomography-based measurements of tissue elasticity," Laser Physics Letters, 10(7), (2013).

[110] M. Singh, R. Raghunathan, V. Piazza, A. M. Davis-Loiacono, A. Cable, T. J. Vedakkan, T. Janecek, M. V. Frazier, A. Nair, C. Wu, I. V. Larina, M. E. Dickinson, and K. V. Larin, "Applicability, usability, and limitations of murine embryonic imaging with optical coherence tomography and optical projection tomography," Biomedical Optics Express, 7(6), 2295-2310 (2016).

[111] J. Li, S. Wang, R. K. Manapuram, M. Singh, F. M. Menodiado, S. Aglyamov, S. Emelianov, M. D. Twa, and K. V. Larin, "Dynamic optical coherence tomography measurements of elastic wave propagation in tissue-mimicking phantoms and mouse cornea in vivo," Journal of Biomedical Optics, 18(12), 121503 (2013).

[112] S. Song, Z. Huang, and R. K. Wang, "Tracking mechanical wave propagation within tissue using phase-sensitive optical coherence tomography: motion artifact and its compensation," Journal of Biomedical Optics, 18(12), 121505 (2013).

[113] S. R. Aglyamov, S. Wang, A. B. Karpiouk, J. Li, M. Twa, S. Y. Emelianov, and K. V. Larin, "The dynamic deformation of a layered viscoelastic medium under surface excitation," Physics in Medicine & Biology, 60(11), 4295-312 (2015).

[114] K. D. Mohan, and A. L. Oldenburg, “Elastography of soft materials and tissues by holographic imaging of surface acoustic waves,” Optics Express, 20(17), 18887-97 (2012).

[115] E. Soczkiewicz, “The penetration depth of Rayleigh surface waves,” Acustica, 82(2), 380-382 (1996).

[116] J. Keenan, D. F. Orr, and B. K. Pierscionek, “Patterns of crystallin distribution in porcine eye lenses,” Molecular Vision, 14(146-47), 1245-1253 (2008).

[117] S. Lerman, S. Zigman, and W. F. Forbes, “Properties of a cryoprotein in the ocular lens,” Biochemical and Biophysical Research Communications, 22(1), 57-61 (1966).

[118] M. Posner, M. Hawke, C. LaCava, C. J. Prince, N. R. Bellanco, and R. W. Corbin, “A proteome map of the zebrafish (Danio rerio) lens reveals similarities between zebrafish and mammalian crystallin expression,” Molecular Vision, 14, 806 (2008).

[119] K. R. Heys, M. G. Friedrich, and R. J. Truscott, “Presbyopia and heat: changes associated with aging of the human lens suggest a functional role for the small heat shock protein, α-crystallin, in maintaining lens flexibility,” Aging Cell, 6(6), 807-815 (2007).

[120] M. N. Miranda, “Environmental temperature and senile cataract,” Transactions of the American Ophthalmological Society, 78, 255 (1980).

[121] E. Asmussen, F. Bonde-Petersen, and K. Jørgensen, “Mechano-elastic properties of human muscles at different temperatures,” Acta Physiologica Scandinavica, 96(1), 83-93 (1976).

[122] S. M. Elmore, L. Sokoloff, G. Norris, and P. Carmeci, “Nature of "imperfect" elasticity of articular cartilage,” Journal of Applied Physiology, 18(2), 393-396 (1963).

[123] P.-H. Tsui, C.-C. Huang, C.-C. Chang, S.-H. Wang, and K. K. Shung, “Feasibility study of using high-frequency ultrasonic Nakagami imaging for characterizing the cataract lens in vitro,” Physics in Medicine and Biology, 52(21), 6413 (2007).

[124] P. A. Asbell, L. Dualan, J. Mindel, D. Brocks, M. Ahmad, and S. Epstein, “Age-related cataract,” The Lancet, 365(9459), 599-609 (2005).

[125] D. C. Beebe, N. M. Holekamp, and Y.-B. Shui, “Oxidative damage and the prevention of age-related cataracts,” Ophthalmic Research, 44, 155-165 (2010).

[126] X.-L. Cui, and M. Lou, “The effect and recovery of long-term H_2O_2 exposure on lens morphology and biochemestry,” Experimental Eye Research, 57, 157-167 (1993).

[127] S. J. McGinty, and R. J. W. Truscott, “Presbyopia: The First Stage of Nuclear Cataract? ,” Ophthalmic Research, 38, 137-148 (2006).

[128] R. Michael, and A. J. Bron, “The ageing lens and cataract: a model of normal and pathological ageing,” Philosophical Transactions of the Royal Society B: Biological Sciences, 366(1568), 1278-1292 (2011).

[129] A. Taylor, and K. J. A. Davies, “Protein Oxidation and Loss of Protease Activity May Lead to Cataract Formation in the Aged Lens,” Free Radical Biology and Medicine, 3(6), 371-377 (1987).

[130] R. J. Truscott, “Age-related nuclear cataract—oxidation is the key,” Experimental Eye Research, 80, 709-725 (2005).

[131] N. J. Kleiman, and A. Spector, “DNA Single-Strand Breaks in Human Lens Epithelial-Cells from Patients with Cataract,” Current Eye Research, 12(5), 423-431 (1993).

[132] S. H. Heruye, L. N. M. Nkenyi, N. U. Singh, D. Yalzadeh, K. K. Ngele, Y.-F. Njie-Mbye, S. E. Ohia, and C. A. Opere, “Current trends in the pharmacotherapy of cataracts,” Pharmaceuticals, 13(15), 1-41 (2020).

[133] A. Kamei, “Glutathione levels of the human crystalline lens in aging and its antioxidant effect against the oxidation of lens proteins,” Biological and Pharmaceutical Bulletin, 16(9), 870-5 (1993).

[134] L. Schulte, J. Mao, J. Reitz, S. Sreeramulu, D. Kudlinzki, V. V. Hodirnau, J. Meier-Credo, K. Saxena, F. Buhr, J. D. Langer, M. Blackledge, A. S. Frangakis, C. Glaubitz, and H. Schwalbe, “Cysteine oxidation and disulfide formation in the ribosomal exit tunnel,” Nature Communications, 11(1), 5569 (2020).

[135] F. J. Giblin, B. Chakrapani, and V. N. Reddy, “Glutathione and lens epithelial function,” Investigative Ophthalmology & Visual Science, 15(5), 381-93 (1976).

[136] F. J. Giblin, J. P. Mccready, J. R. Reddan, D. C. Dziedzic, and V. N. Reddy, "Detoxification of H2o2 by Cultured Rabbit Lens Epithelial-Cells - Participation of the Glutathione Redox Cycle," Experimental Eye Research, 40(6), 827-840 (1985).

[137] D. L. Williams, "Oxidation, antioxidants and cataract formation: a literature review," Veterinary Ophthalmology, 9(5), 292-298 (2006).

[138] L. Packer, E. H. Witt, and H. J. Tritschler, "Alpha-lipoic acid as a biological antioxidant," Free Radical Biology and Medicine, 19(2), 227-250 (1995).

[139] E. Kan, E. Kilickan, A. Ayar, and R. Colak, "Effects of two antioxidants; alpha-lipoic acid and fisetin against diabetic cataract in mice," International Ophthalmology, 35(1), 115-120 (2015).

[140] S. B. Khan, R. Choudhary, P. K. Vishwakarma, A. Singh, J. Shree, and S. H. Bodakhe, "Protective effect of alpha-lipoic acid on progression of cataract formation in fructose-induced experimental cataract," PharmaNutrition, 5(4), 127-132 (2017).

[141] M. Kojima, L. Sun, I. Hata, Y. Sakamoto, H. Sasaki, and K. Sasaki, "Efficacy of α-lipoic acid against diabetic cataract in rat," Japanese Journal of Ophthalmology, 51(1), 10-13 (2007).

[142] Y. Li, Y.-Z. Liu, J.-M. Shi, and S.-B. Jia, "Alpha lipoic acid protects lens from H2O2-induced cataract by inhibiting apoptosis of lens epithelial cells and inducing

activation of anti-oxidative enzymes," Asian Pacific Journal of Tropical Medicine, 6(7), 548-551 (2013).

[143] I. Maitra, E. Serbinova, H. Trischler, and L. Packer, "α-Lipoic acid prevents buthionine sulfoximine-induced cataract formation in newborn rats," Free Radical Biology and Medicine, 18(4), 823-829 (1995).

[144] D. L. Williams, "Effect of Oral Alpha Lipoic Acid in Preventing the Genesis of Canine Diabetic Cataract: A Preliminary Study," Veterinary Sciences, 4(1), (2017).

[145] C. Wu, S. R. Aglyamov, H. Zhang, and K. V. Larin, "Measuring the elastic wave velocity in the lens of the eye as a function of intraocular pressure using optical coherent elastography," Quantum Electronics, 49(1), 20-24 (2019).

[146] M. McNamara, and R. C. Augusteyn, "The effects of hydrogen peroxide on lens proteins: a possible model for nuclear cataract," Experimental Eye Research, 38(1), 45-56 (1984).

[147] M. Ozgokce, M. Batur, M. Alpaslan, A. Yavuz, A. Batur, E. Seven, and H. Arslan, "A comparative evaluation of cataract classifications based on shear-wave elastography and B-mode ultrasound findings," Journal of Ultrasound, 22(4), 447-452 (2019).

[148] S. D. Varma, K. R. Hegde, and S. Kovtun, "Oxidative damage to lens in culture: Reversibility by pyruvate and ethyl pyruvate," Ophthalmologica, 220(1), 52-57 (2006).

[149] A. Spector, G. M. Wang, R. R. Wang, W. H. Garner, and H. Moll, "The prevention of cataract caused by oxidative stress in cultured rat lenses. I. H2O2 and photochemically induced cataract," Current Eye Research, 12(2), 163-79 (1993).

[150] E. Lanchares, R. Navarro, and B. Calvo, "Hyperelastic modelling of the crystalline lens: Accommodation and presbyopia," Journal of Optometry, 5(3), 110-120 (2012).

[151] R. A. Schachar, R. W. Chan, and M. Fu, "Viscoelastic properties of fresh human lenses under 40 years of age: implications for the aetiology of presbyopia," British Journal of Ophthalmology, 95(7), 1010-1013 (2011).

[152] Y. Li, J. Zhu, J. J. Chen, J. X. Yu, Z. Jin, Y. S. Miao, A. W. Browne, Q. F. Zhou, and Z. P. Chen, "Simultaneously imaging and quantifying in vivo mechanical properties of crystalline lens and cornea using optical coherence elastography with acoustic radiation force excitation," APL Photonics, 4(10), (2019).

[153] Q. M. Wang, Y. Zhu, M. Shao, H. M. Lin, S. P. Chen, X. Chen, A. Alizad, M. Fatemi, and X. Y. Zhang, "In vivo assessment of the mechanical properties of crystalline lenses in a rabbit model using ultrasound elastography: Effects of ultrasound frequency and age," Experimental Eye Research, 184, 258-265 (2019).

[154] Y. Xiang, T. Fu, Q. F. Xu, W. Chen, Z. Q. Chen, J. M. Guo, C. H. Deng, A. Manyande, P. Wang, H. Zhang, X. B. Tian, and J. M. Wang, "Quantitative analysis of internal components of the human crystalline lens during accommodation in adults," Scientific Reports, 11(1), (2021).

[155] G. H. Reggiani Mello, and R. R. Krueger, “Femtosecond laser photodisruption of the crystalline lens for restoring accommodation,” International Ophthalmology Clinics, 51(2), 87-95 (2011).

[156] H. Zhang, M. Singh, A. Nair, K. V. Larin, and S. R. Aglyamov, “Elasticity changes in the crystalline lens during oxidative damage and the antioxidant effect of alpha-lipoic acid measured by optical coherence elastography,” Photonics, 8(6), 207 (2021).

[157] Z. L. Han, J. S. Li, M. Singh, C. Wu, C. H. Liu, S. Wang, R. Idugboe, R. Raghunathan, N. Sudheendran, S. R. Aglyamov, M. D. Twa, and K. V. Larin, “Quantitative methods for reconstructing tissue biomechanical properties in optical coherence elastography: a comparison study,” Physics in Medicine and Biology, 60(9), 3531-3547 (2015).

[158] Z. L. Han, M. Singh, S. R. Aglyamov, C. H. Liu, A. Nair, R. Raghunathan, C. Wu, J. S. Li, and K. V. Larin, “Quantifying tissue viscoelasticity using optical coherence elastography and the Rayleigh wave model,” Journal of Biomedical Optics, 21(9), (2016).

[159] L. F. Garner, and G. Smith, “Changes in equivalent and gradient refractive index of the crystalline lens with accommodation,” Optometry and Vision Science, 74(2), 114-119 (1997).

[160] M. A. Choma, A. K. Ellerbee, C. H. Yang, T. L. Creazzo, and J. A. Izatt, “Spectral-domain phase microscopy,” Optics Letters, 30(10), 1162-1164 (2005).

[161] R. K. Manapuram, V. G. R. Manne, and K. V. Larin, "Phase-sensitive swept source optical coherence tomography for imaging and quantifying of microbubbles in clear and scattering media," Journal of Applied Physics, 105(10), (2009).

[162] M. D. Twa, J. S. Li, S. Vantipalli, M. Singh, S. Aglyamov, S. Emelianov, and K. V. Larin, "Spatial characterization of corneal biomechanical properties with optical coherence elastography after UV cross-linking," Biomedical Optics Express, 5(5), 1419-1427 (2014).

[163] F. Zvietcovich, A. Nair, Y. S. Ambekar, M. Singh, S. R. Aglyamov, M. D. Twa, and K. V. Larin, "Confocal air-coupled ultrasonic optical coherence elastography probe for quantitative biomechanics," Optics Letters, 45(23), 6567-6570 (2020).

[164] F. Zvietcovich, J. N. Yao, J. P. Rolland, and K. J. Parker, "Experimental classification of surface waves in optical coherence elastography," Optical Elastography and Tissue Biomechanics III, 9710, (2016).

[165] W. M. Ewing, W. S. Jardetzky, and F. Press, [Elastic waves in layered media] Graw-Hill Book Company, Inc, (1957).

[166] B. W. Shaffer, "Generalized plane strain of pressurized orthotropic tubes," Journal of Engineering for Industry, 87(3), 337-343 (1965).

[167] Y. Ambekar, M. Singh, J. T. Zhang, A. Nair, S. R. Aglyamov, G. Scarcelli, and K. V. Larin, "Multimodal quantitative optical elastography of the crystalline lens with optical coherence elastography and Brillouin microscopy," Biomedical Optics Express, 11(4), 2041-2051 (2020).

[168] F. M. Elrefaei, M. S. Hassan, I. H. Ibrahim, and R. N. Afify, “Characterization of conductivity and viscosity for rabbit's eye lens following ultrasound exposure,” Journal of Global Biosciences, 4(8), 3229-3237 (2015).

[169] A. Sorsby, J. Stone, G. A. Leary, and M. Sheridan, “Changes in the depth of the anterior chamber and in the radius of curvature of the front surface of the lens during growth. Observations on the rabbit,” British Journal of Ophthalmology, 44, 467-71 (1960).

Journal Publications with Authorship

Zhang, H., Wu, C., Singh, M., Nair, A., Aglyamov, S. R., & Larin, K. V. (2019). Optical coherence elastography of cold cataract in porcine lens. In *Journal of biomedical optics*, *24*(3), 036004.

Zhang, H., Singh, M., Nair, A., Larin, K. V., & Aglyamov, S. R. (2021, June). Elasticity Changes in the Crystalline Lens during Oxidative Damage and the Antioxidant Effect of Alpha-Lipoic Acid Measured by Optical Coherence Elastography. In *Photonics* (Vol. 8, No. 6, p. 207).

Zhang, H., Singh, M., Zvietcovich, F., Larin, K. V., & Aglyamov, S. R. (2022, January). Age-Related Changes in the Viscoelasticity of Rabbit Lens Characterized by Surface Wave Dispersion Analysis. In *Quantum Electronics* (Accepted).

Liu, C. H., Nevozhay, D., Zhang, H., Das, S., Schill, A., Singh, M., ... & Larin, K. V. (2019). Longitudinal elastic wave imaging using nanobomb optical coherence elastography. *Optics letters*, *44*(12), 3162-3165.

Wu, C., Aglyamov, S. R., Zhang, H., & Larin, K. V. (2019). Measuring the elastic wave velocity in the lens of the eye as a function of intraocular pressure using optical coherent elastography. *Quantum Electronics*, *49*(1), 20.